# DIFFRACTION OF MICROWAVES

# DIFFRACTION OF MICROWAVES ALONG THE AXIS OF PROPAGATION BEHIND CONDUCTING AND DIELECTRIC RODS AND A PLASTIC PRISM

By

WILLARD ALEXANDER YOUNG, B.Sc.

A Thesis

Submitted to the Faculty of Graduate Studies

in Partial Fulfilment of the Requirements

for the Degree

Master of Science

McMaster University

May 1963

MASTER OF SCIENCE (1963) McMASTER UNIVERSITY
(Physics) Hamilton, Ontario.

TITLE: Diffraction of Microwaves Along the Axis of Propagation Behind Conducting and Dielectric Rods and a Plastic Prism.

AUTHOR: Willard Alexander Young, B.Sc. (McMaster University).

SUPERVISOR: Professor A. B. McLay.

NUMBER OF PAGES: vi, 42.

SCOPE AND CONTENTS: The first chapter of this thesis consists of a general introduction and a brief description of previous work done in this same laboratory. Also included is a preliminary description of the present experiment. This is followed, in Chapter 2, by a detailed description of the experimental apparatus. The third and last chapter contains a description of the procedure used in obtaining results, as well as the results themselves. Measurements were made of the diffraction patterns of a plastic prism, and five rods in a total of nine different cases. In all cases, the intensity measurements were made along the axis of propagation of the incident beam behind the diffracting object. A polarization normal to the axis of the rods was used. Theoretical calculations were made in three cases, and compared with the experimental results.

## ACKNOWLEDGEMENTS

The author wishes to express his sincere gratitude to Professor A. B. McLay for his valuable direction and assistance throughout the course of the experiment. Appreciation is expressed to Mr. P. Leung who constructed some of the equipment used in this project.

Financial aid from the Physics Department in the form of a research assistantship, and from the National Research Council in the form of a summer assistantship as part of a continued grant-in-aid to Professor McLay are also gratefully acknowledged.

TABLE OF CONTENTS


| | | PAGE |
|---|---|---|
| Descriptive Note | | ii |
| Acknowledgements | | iii |
| List of Illustrations | | v |
| List of Plates | | vi |
| Chapter 1. Introduction | | |
| 1-1 | Early Developments | 1 |
| 1-2 | Microwave Optics | 2 |
| 1-3 | Scope of the Experiment | 3 |
| Chapter 2. Experimental Arrangement | | |
| 2-1 | The Microwave Transmitter | 6 |
| 2-2 | The Probe and Track Assembly | 8 |
| 2-3 | The Amplifier and Recorder | 10 |
| 2-4 | The Microwave Darkroom | 11 |
| 2-5 | The Diffracting Cylinders and Prism | 14 |
| Chapter 3. Experimental Procedure and Results | | |
| 3-1 | Transmitter Stability | 15 |
| 3-2 | Geometry of Diffraction Experiment and Placing of Rods | 16 |
| 3-3 | Procedure in taking Runs | 18 |
| 3-4 | Analysis of Results | 19 |
| 3-5 | 1 Inch Brass Rod | 21 |
| 3-6 | The 1½ Inch Foil-Covered Semicylinders | 22 |
| 3-7 | The 1 Inch Lucite Circular Cylinder | 23 |
| 3-8 | The 1½ Inch Lucite Circular Cylinder | 27 |
| 3-9 | The 1½ Inch Lucite Semicylinder | 28 |
| 3-10 | The Dielectric Prism | 29 |
| 3-11 | Effect of Probe Orientation on Observed Patterns | 31 |
| 3-12 | Conclusions | 34 |
| Appendix. The Theoretical Field Equations | | 37 |
| References. | | 42 |

## LIST OF ILLUSTRATIONS


| FIGURE | DESCRIPTION | AFTER PAGE |
|---|---|---|
| 1 | Microwave Transmitter | 7 |
| 2 | Microwave Probe | 8 |
| 3 | Component of Field Detected by Probe | 8 |
| 4 | Probe and Track Assembly | 10 |
| 5 | Arrangement of Apparatus | 12 |
| 6 | Sample of Incident Field | 20 |
| 7 | 1 Inch Brass Rod | 21 |
| 8 | Foil Covered Lucite 1½ Inch Semicylinder | 22 |
| 9 | Foil Covered Lucite 1½ Inch Semicylinder | 23 |
| 10 | 1 Inch Lucite Rod | 23 |
| 11 | Refraction of Rays by Lucite Rod | 24 |
| 12 | Calculated Values of Intensity for 1 Inch Lucite Rod | 27 |
| 13 | 1½ Inch Lucite Rod | 27 |
| 14 | Calculated Values of Intensity for 1½ Inch Lucite Rod | 28 |
| 15 | 1½ Inch Lucite Semicylinder | 29 |
| 16 | 1½ Inch Lucite Semicylinder | 29 |
| 17 | Refraction of Rays by Lucite Semicylinder | 29 |
| 18 | Selectron Prism | 30 |
| 19 | Selectron Prism | 30 |
| 20 | Geometry of Diffraction Experiment | 41 |

## LIST OF PLATES


| PLATE | DESCRIPTION | AFTER PAGE |
|---|---|---|
| 1 | Track Drive Mechanism | 11 |
| 2 | Amplifier and Recorder | 11 |
| 3 | Darkroom: Transmitting End | 13 |
| 4 | Darkroom: Probe End | 13 |

# CHAPTER 1

# INTRODUCTION

## 1-1 Early Developments

The last hundred years or so have seen the expansion of the electromagnetic spectrum on both sides of the visible region, from radio to gamma rays. The first experimental evidence of a relationship between light and electricity and magnetism was obtained by Michael Faraday near the middle of the last century. He observed the rotation of the plane of polarization of a light beam passed through a piece of lead glass in a direction parallel to an applied magnetic field. This was soon followed by Maxwell's unexpected discovery of the similarity of the velocity of light and the velocity of his theoretical "electromagnetic waves." Heinrich Hertz proved the existence of Maxwell's electromagnetic waves experimentally using an induction coil, spark gap, and two metal sheets as a generator.

Hertz's discovery has led to the development of radio equipment utilizing electromagnetic or "Hertzian" waves from kilometer to centimeter wavelengths. It is only recently, however, that the gap between "radio" and the far infrared has been closed by the development of special

oscillators.

## 1-2 Microwave Optics

Waves throughout the entire spectrum are fundamentally identical except for wavelength and frequency. They all obey the same laws of diffraction and interference. It is possible to demonstrate these effects in any part of the spectrum, in principle at least. The phenomena of diffraction and interference of light were well known in the early nineteenth century, and were explained, first by Young and later by Fresnel, in terms of a wave theory. Quite thorough investigations were made, and most of the observed phenomena were satisfactorily accounted for.

Because of the wavelengths involved in the visible region, the diffraction patterns are always observed at a large distance (in terms of wavelengths) from the diffracting object. Accurate studies of effects in the immediate vicinity of the object are extremely difficult, if not impossible to make.

Since oscillators are now available which operate in the centimeter region, studies can be made of effects close to the object. In addition, the objects used may be made comparable to the wavelength in size. As a result, classical diffraction theory is continually being augmented and extended by new knowledge of the near-field region. Approximations for small wavelength, which simplified the theory in the optical case, become invalid in the microwave

case. This complicates the theory, but provides an excellent test of its ability to describe strongly localized effects. The calculation of a diffraction pattern becomes essentially a problem of solving Maxwell's equations with the proper boundary conditions.

## 1-3 Scope of the Experiment

Considerable work has been done by other experimenters in this laboratory on the diffraction patterns of conducting and dielectric cylinders, all at 3.2 cm. Wiles (1) obtained intensity and phase measurements about a 1 inch brass rod and a 1 inch hard rubber rod, with the polarization parallel to the axis of each rod. Runs were taken perpendicular to the axis of propagation at several distances behind the rods, and results for the conducting case were compared with theory. Keys (2) studied the diffraction patterns of 1 inch brass, hard rubber, and lucite cylinders, using a polarization perpendicular to the axis of the rods. Results for the lucite rod were compared with theoretical calculations by Froese and Wait (3). Lucite and tenite 1 inch diameter cylinders were studied by Subbarao (4) using parallel polarization, and the patterns were compared with theoretical calculations of Froese and Wait (3). Subbarao (5) also studied, experimentally, the diffraction patterns of a $1\frac{1}{2}$ inch lucite cylinder, and of a $1\frac{1}{2}$ inch lucite semicylinder with plane face toward and away from the source. Jordan (6)

reinvestigated the region close to the semicylinder in the above two cases, and also with the plane face along the propagation direction. In addition, he investigated these three cases with the semicylinder coated with aluminum foil. As in the work of Subbarao, the incident field was polarized parallel to the axis of the cylinder. In all cases runs were taken transverse to the incident beam.

Extensive investigations of diffraction and evanescent wave effects have also been conducted in this laboratory using a large plastic prism described in section 2-5. Diffraction patterns of wedges have been studied by Jordan (7), Dignum (8), and Hedgecock (9) using various orientations of the prism. The evanescent wave behind a totally internally reflecting surface has been investigated by Jordan, Leung (10), and in considerable detail by Hedgecock. Before the plastic prism was available, studies had been made of the evanescent wave, and diffraction of wedges by Kneeland (11) using a prism of paraffin wax. In all cases the direction of the run made an angle with the incident beam of either 45° or 90°.

In the present experiment, field intensity measurements were made along the axis of propagation behind cylinders of brass and lucite, as well as behind semi-cylinders of lucite, and foil-covered lucite. Axial runs were also taken behind the dielectric prism with the hypotenuse face toward, and away from the source. The polarization was perpendicular to the axis of each rod,

and to the apex edge of the prism.

Field measurements made along the axis are easier to analyse than off-axis measurements. Because the latter would involve radiation coming from the object as well as directly from the horn, the directional characteristics of the probe would have to be considered. The electric vector of the incident field would be parallel to the probe axis as usual, but that of the reradiated, or scattered field would not be. Only a component of this field would be detected (see Fig. 3), and that component would depend on the position of the probe relative to the rod. The component detected would be the y component as desired provided the probe characteristics had the ideal cosine form as indicated in Fig. 3. If the probe characteristics were not ideal and symmetrical, the field value obtained would not be truly indicative of $E_y$ in all positions. As long as the probe remains on the axis of propagation, however, the electric field of all radiation incident on the probe will be practically parallel to the probe axis. In addition, by considering fields only along the axis of propagation, the theoretical expressions simplify considerably so that calculations are not prohibitively involved. This then allows a comparison to be made of three cases with a theoretical expression given by Froese and Wait (3). The cases studied theoretically were the 1 inch brass rod, and the two lucite circular cylinders.

# CHAPTER 2

## EXPERIMENTAL ARRANGEMENT

### 2-1 The Microwave Transmitter

While somewhat involved in practice, the experimental arrangement for a diffration experiment is quite simple in principle. It consists essentially of a source of radiation, a diffracting object, and a detecting device.

The source of 3.2 cm. microwave radiation consists of a Varian VA-242E reflex klystron pretuned to 9.375 kMc/sec., and capable of delivering 725 mw. of power. An FXR Model Z819B klystron power supply provides the necessary tube voltages, as well as the 1 kc./sec. square-wave modulation. The frequency is quite sensitive to the temperature of the klystron. Thus, in order to eliminate the effects of random air currents around the tube, a blower is used to provide a steady stream of air. As well as stabilizing the frequency, this keeps the klystron cool. From the klystron, the microwave power is fed, in the $TE_{10}$ mode, through a short section of RG-52/U wave guide to the pyramidal horn radiator.

The horn, constructed by C. E. Jordan in this laboratory, is made of brass with a 10.1 cm. square aperture. From the apex to the aperture, the distance is 38.7 cm. in the H-plane, and 33.4 cm. in the E-plane, giving H and E-plane angles of 15 and 17 respectively. The horn was designed to have a broad radiation pattern in both the vertical and horizontal planes in order to approximate, as nearly as possible, to the desired plane wave condition. This was an important consideration in the previous work already mentioned, since probe runs normal to, or at a 45 angle to the propagation direction were made. In the present work, the incident field may be considered perfectly plane since probe runs are taken along the axis of propagationc and the diffracting objects are small enough to subtend quite small angles at the horn (less than 27' of arc for the cylinders.)

In the waveguide between klystron and horn is a variable flap attenuator, used to adjust the rf. power level, and a directional coupler. It is through this latter component that the small amount of power necessary for monitoring and frequency measurement is obtained. Connected to the directional coupler is the frequency meter, which is followed by a 1N23C crystal diode detector inserted in the waveguide. A 0-50 a meter is connected to the diode as the power indicator. Fig. 1 illustrates the arrangement of the transmitter.

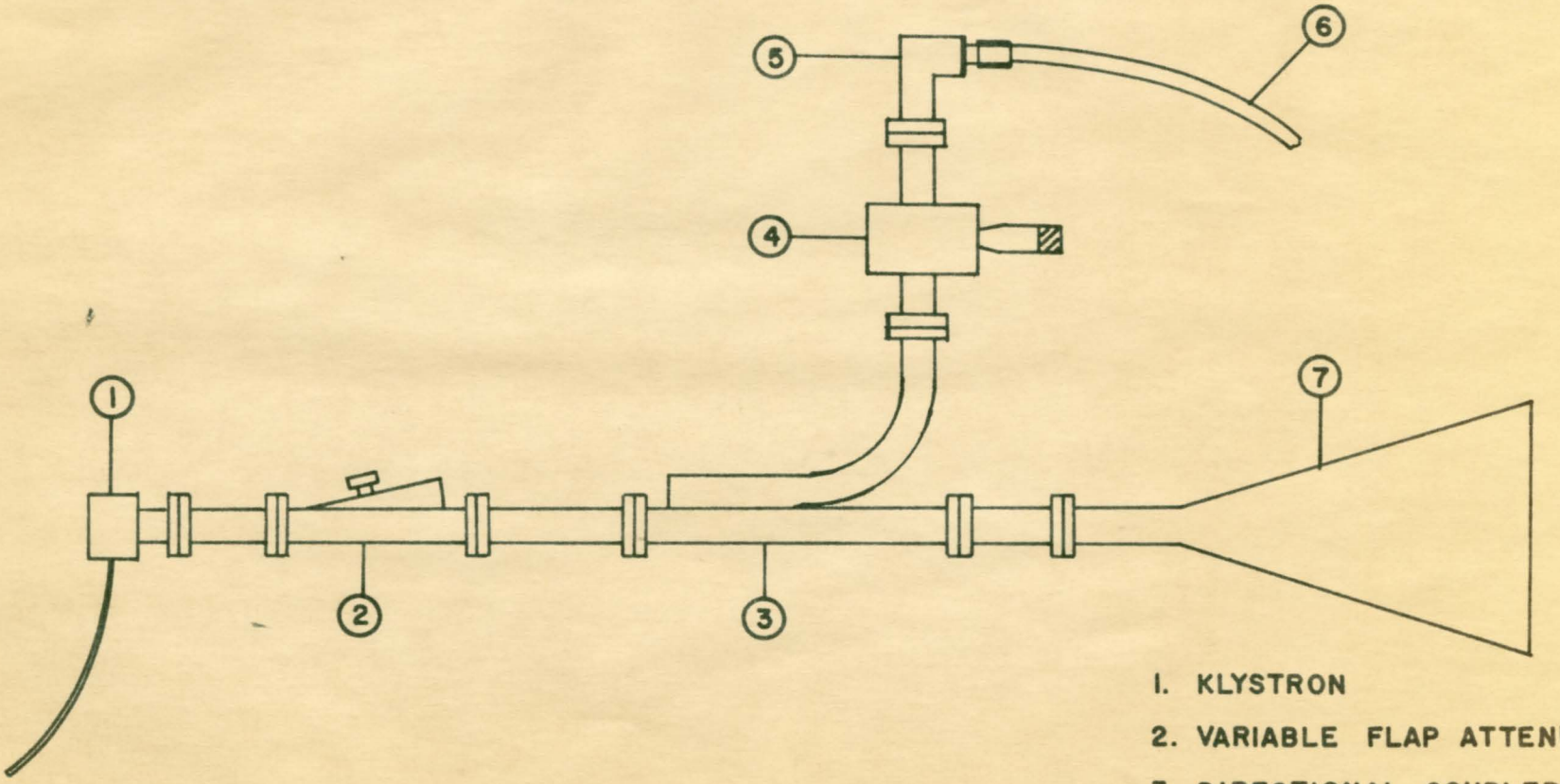


1. KLYSTRON
2. VARIABLE FLAP ATTENUATOR
3. DIRECTIONAL COUPLER
4. FREQUENCY METER
5. CRYSTAL DETECTOR
6. COAXIAL CABLE TO MONITORS
7. HORN

FIG. 1: MICROWAVE TRANSMITTER

## 2-2 The Probe and Track Assembly

The field intensity behind the diffracting objects was determined by means of a small probe consisting of a 1N833 computer diode. The diode, 0.7 cm. long and 0.25 cm. in diameter, is mounted on the end of a 0.55 cm. outside diameter glass tube as shown in Fig. 2, and acts as both antenna and demodulator. The leads are bent sharply at the diode to keep the overall length as short as possible, and are held in place by a drop of paraffin wax inside the glass tube. From the diode, the detected signal is carried along 60 cm. of miniature coaxial cable 0.2 cm. overall diameter, where it is then carried by standard RG-58/U cable to the amplifier and recorder.

The length of the probe itself becomes an important consideration in the case of horizontal polarization, since it is mounted normal to the diffracting rod. The intensity measured is thus a result of integrating the field over the length of the probe. The probe described is less than $0.22\lambda$ in length, and cannot be made shorter with any presently available diodes. There is, in addition, a directional effect as mentioned in section 1-3. Only the component of the field in the direction of the probe axis will be detected. This component varies as the cosine of the angle between the propagation direction, and the normal to the probe axis, as shown in Fig. 3. As discussed in section 1-3,

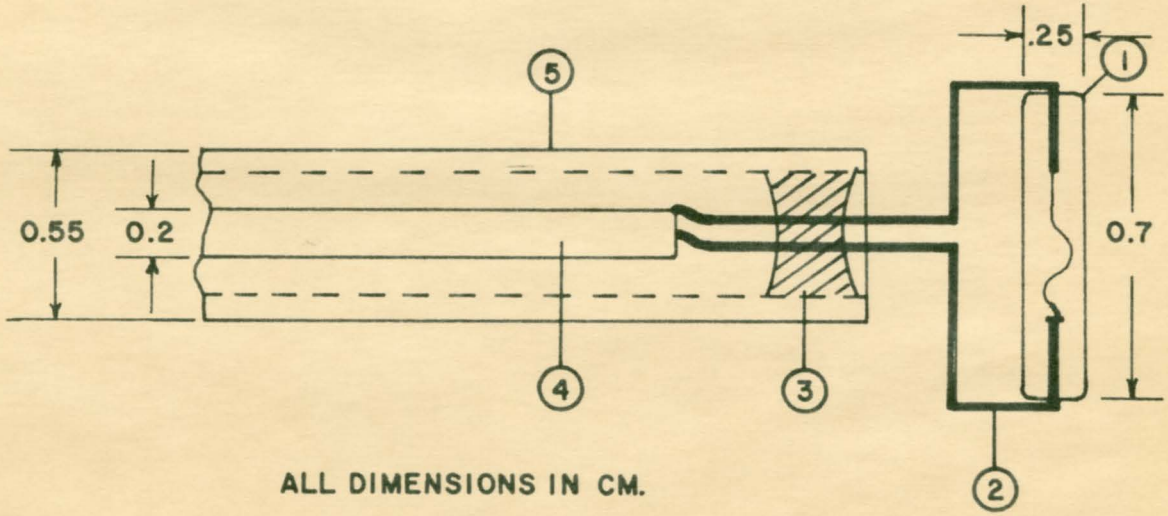


1. IN833 COMPUTER DIODE
2. WIRE LEADS OF DIODE
3. DROP OF PARAFFIN WAX
4. MINIATURE COAXIAL CABLE
5. GLASS TUBE

FIG. 2: MICROWAVE PROBE

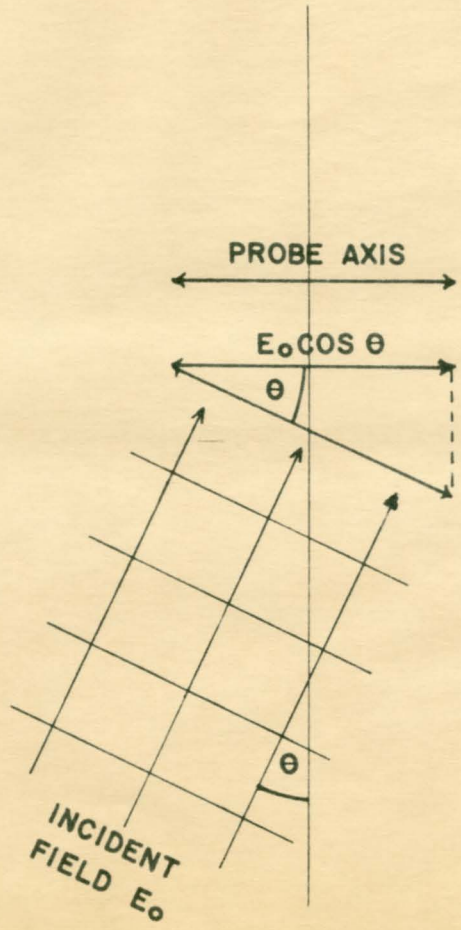


FIG. 3: COMPONENT OF FIELD DETECTED BY PROBE

this problem is eliminated by choosing the axis of propagation for all probe runs.

The probe assembly is supported by a styrofoam column mounted, in turn, on the trolley of an optical bench. Styrofoam was chosen as the support material since it causes negligible disturbance of the field. For greater rigidity, the cross-section of the column was made in the form of a cross, and the upper end is guyed to the trolley with cotton thread. The height of the probe above the floor is nearly 166 cm. or $52\lambda$, the same as that of the horn. The probe and support described are recent modifications made, by t the author, to equipment previously constructed by himself and P. Leung. This equipment is described further below.

The trolley is driven along the optical bench at a speed of 4.0 cm./min. by a steel wire passing over pulleys at the ends of the track, and wound three times around a 4½ inch diameter aluminum drum. The drum is coupled to a 1/25 h.p. Bodine reversible motor through a system of gears having a total ratio of 16000:1. The trolley is prevented from reaching either end of the track by two microswitches which act as safety stops.

In order to relate the pattern produced at the recorder to the position of the probe relative to the diffracting rod, a calibrating device was installed directly at the track. This consists of a meter stick mounted parallel to the track, with fine (30 guage) copper wires wound around the stick every five centimeters. The wires were

inserted in fine knife cuts in the meter stick and were made flush with the top edge by sanding the wood down to expose the top surface of the wires. The wires are connected together by a bus along the lower edge of the stick. A small metal wheel, attached to the trolley, runs along the upper edge of the meter stick making contact with the wires every 5.0 cm. of travel. A relay, operated from a low voltage battery supply, then triggers a second relay through a differentiator circuit. As a result, the recorder input is short-circuited for a very short time, producing a negative calibration pip on the chart. The pip amplitude can be set to any desired value by varying the time constant of the differentiator circuit. The position of each marker has an estimated accuracy of 0.05 cm., and there is no accumulated error in going from one to the next. Fig. 4 illustrates the probe and track assembly, and Plate 1 shows the track drive mechanism.

## 2-3 The Amplifier and Recorder

The 1000 cps. signal from the probe is amplified by a narrow-band amplifier tuned for maximum response at this frequency. The amplifier used in this work was built by P. Leung (10), and is similar to the one originally designed and built by D. Kneeland (11) in this laboratory. Three standard rc-coupled pentode stages are used with a "Twin T" filter network coupled between plate and grid of the second stage. This filter gives the amplifier its narrow band characteristic by coupling all non-resonant signals back to

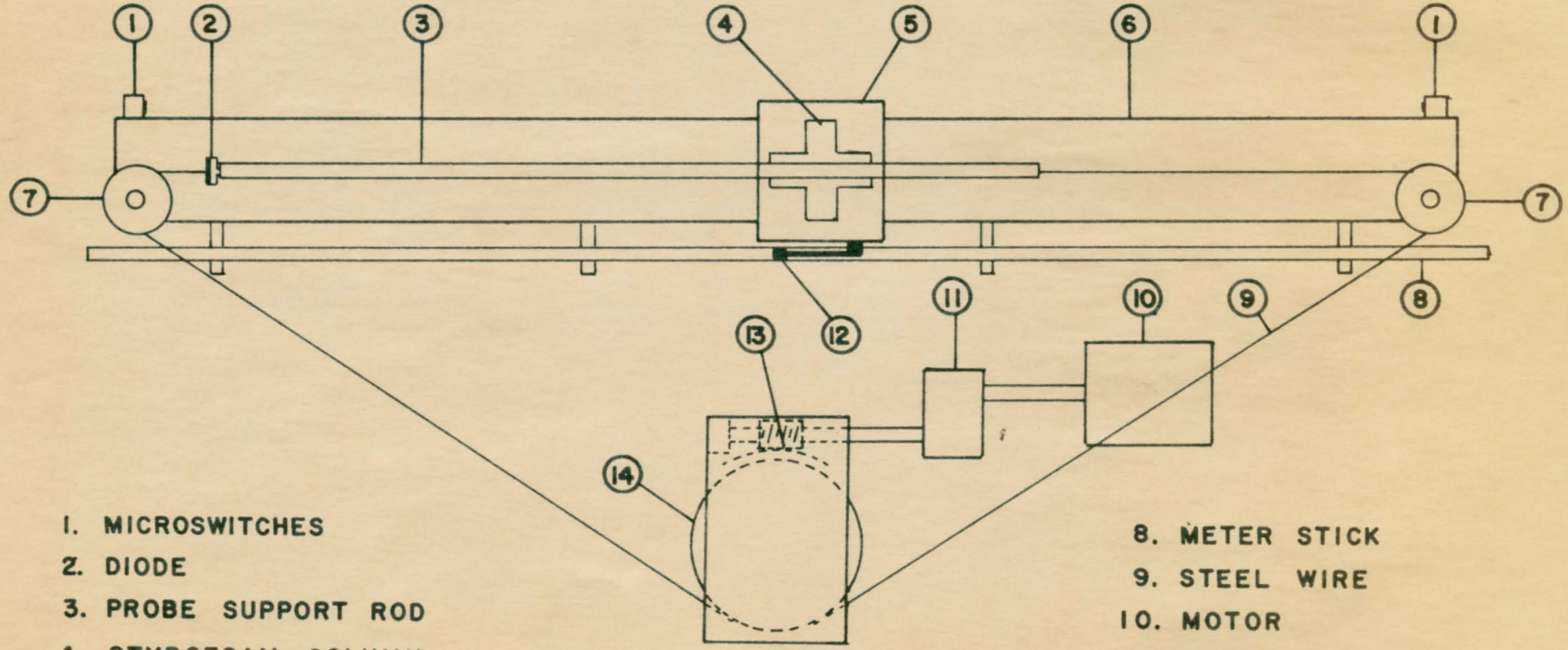


1. MICROSWITCHES
2. DIODE
3. PROBE SUPPORT ROD
4. STYROFOAM COLUMN
5. TROLLEY
6. OPTICAL BENCH
7. PULLEYS
8. METER STICK
9. STEEL WIRE
10. MOTOR
11. GEAR BOX (200:1)
12. CALIBRATION WHEEL
13. WORM DRIVE
14. ALUMINUM DRUM

FIG. 4: PROBE AND TRACK ASSEMBLY

the second stage grid in inverse phase. The third stage is followed by a diode clamp which provides the direct current required by the recorder. The dc pulse signal from the clamping circuit controls the recorder by means of a cathode-follower vacuum tube voltmeter. Power for the amplifier is provided by a Hewlett Packard Model 710 B regulated power supply, and for the vacuum tube voltmeter stage, by a separate 90 volt battery. More detailed descriptions and circuit diagrams are given by Leung and Kneeland.

The recorder is a Brown self balancing potentiometer model 153X17-V-II-III-30 with a 0-5 mv range, and manufactured by the Minneapolis-Honeywell Regulator Co. The chart, divided by a 0-100 scale, was driven at 5.1 cm./min. for all records. All of the equipment described is powered by Sola constant voltage transformers type K0291. Two separate transformers are used, one for the transmitter, and one for the amplifier, recorder, and track. The recorder and amplifier are shown in plate 2.

## 2-4 The Microwave Darkroom

In order to reduce reflections and interference from the walls, pipes, and other objects in the laboratory, a "microwave darkroom" was constructed by the author, using microwave hair absorber obtained from Sponge Rubber Products Co., Shelton, Conn. Thirty-five sections of absorber, each 2 ft. square, were mounted directly on the back wall of

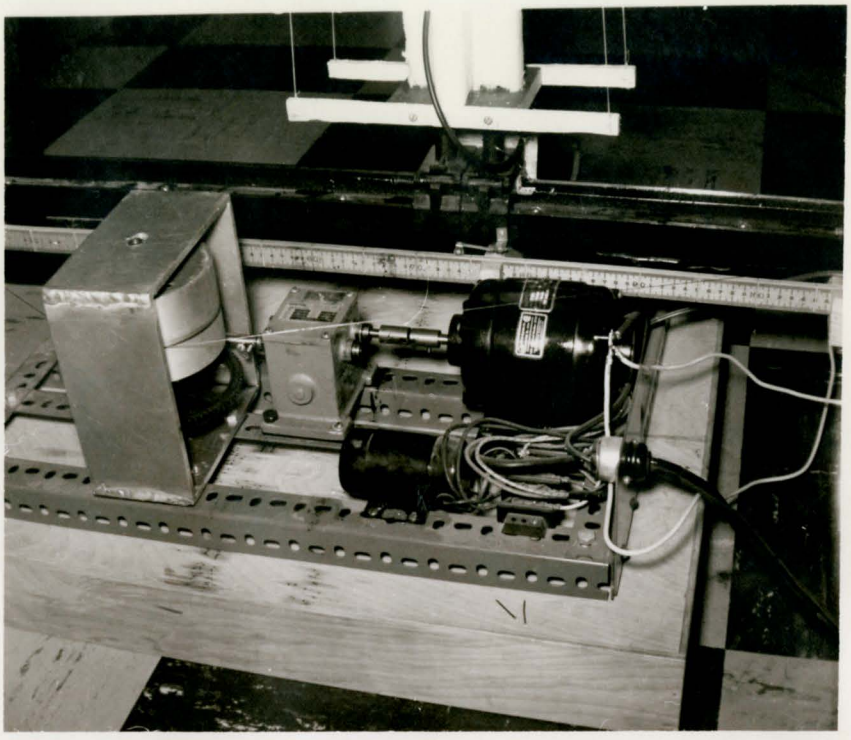

PLATE 1: TRACK DRIVE MECHANISM

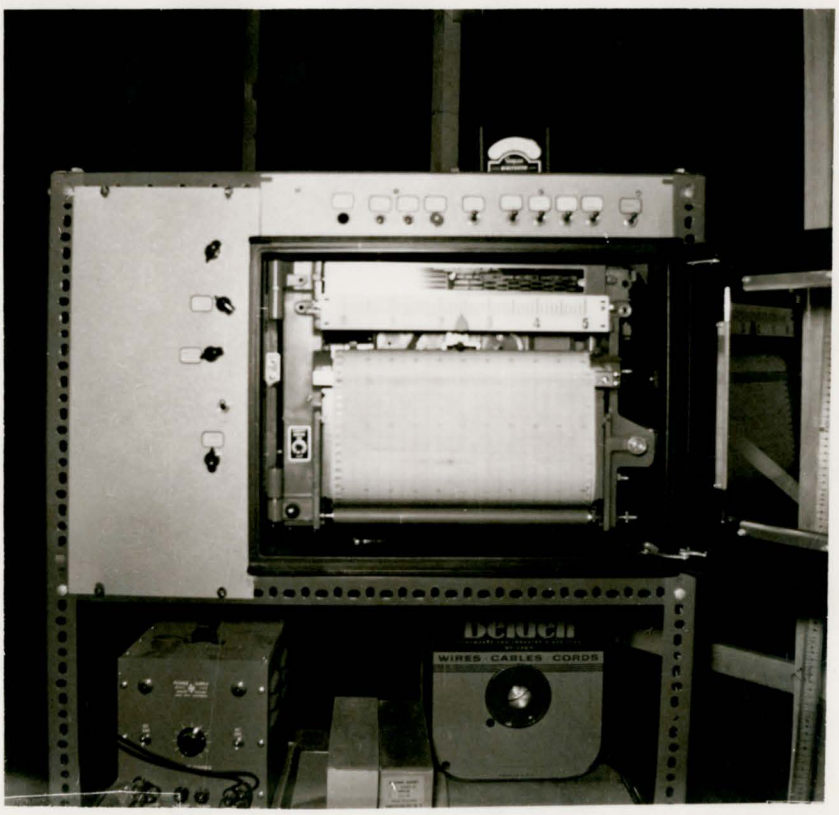


PLATE 2: AMPLIFIER AND RECORDER

the room, covering an area 10 ft. by 14 ft. The left wall of the darkroom (looking from the horn) was made by mounting 57 sections of absorber on a framework of wood. The resulting wall is 10 ft. high and 24 ft. long, with a 2 ft. by 6 ft. doorway at the transmitting end. The front wall (at the horn end) was also constructed on a framework of wood, and is 10 ft. by 10 ft. in size. The remaining, or right hand wall, is similar in size to the left wall, but was constructed partly in the manner of the back wall, and partly in the manner of the left side wall. With the working area enclosed to this extent with absorber, small adjustments in the position of the walls have only a small effect on the field pattern. Previous workers, using less absorber, found the position of the walls to be quite critical. Fig. 5 illustrates the arrangement of the walls of the darkroom.

Over the enclosed area of the darkroom are several steel beams and metal pipes which were covered by hanging, on each one, a "curtain" or baffle of hair absorber. There is also a wooden railing near the back of the room which was covered by a wall of absorber two sections high, and 5½ sections long running parallel to the back wall. This is illustrated in Fig. 5 and can also be seen in Plate 4. With the horizontal polarization used in this experiment, it was expected that the floor and ceiling would be of considerable importance in determining the incident field pattern. Shielding of the forementioned metal objects was

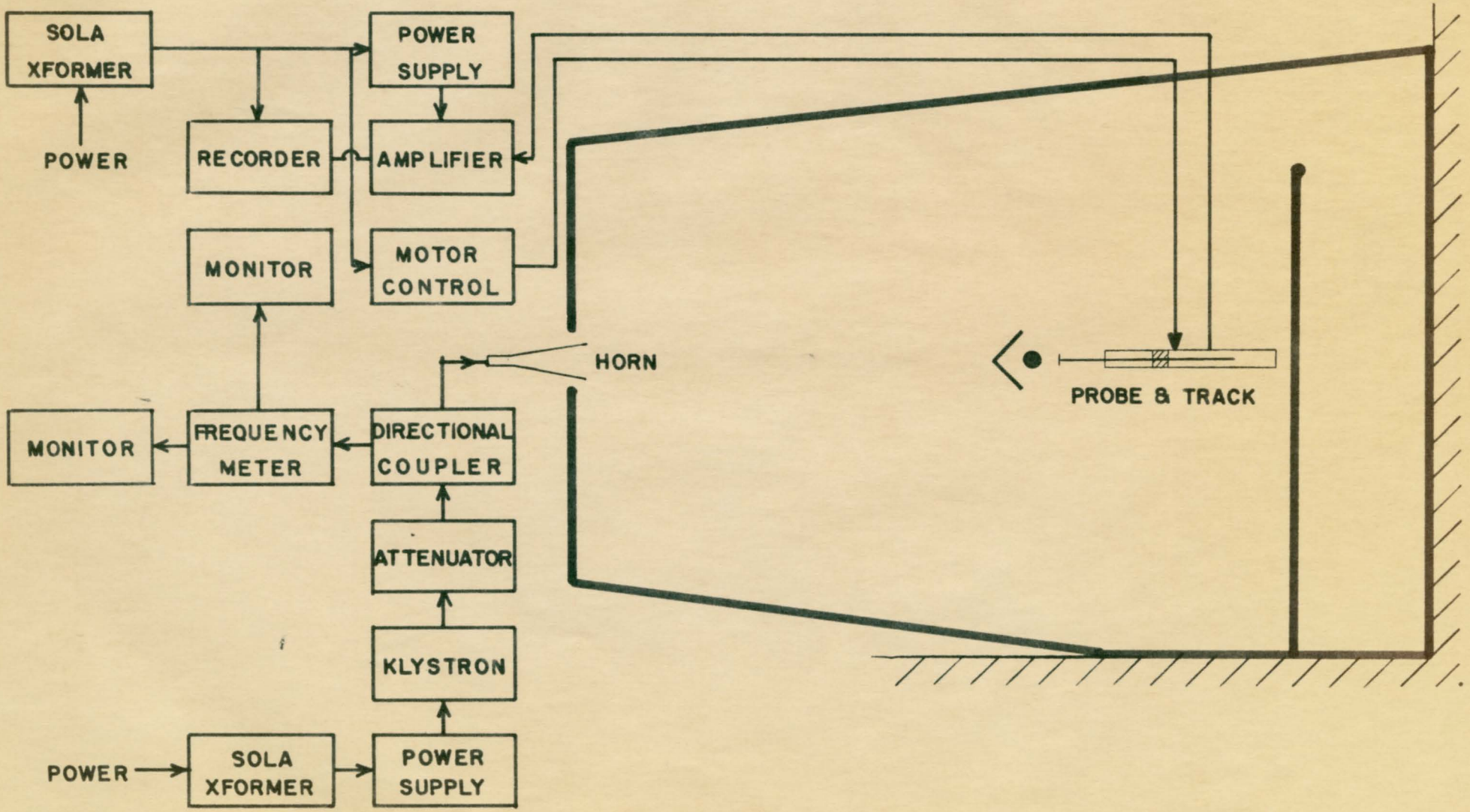


FIG. 5: ARRANGEMENT OF APPARATUS

indeed found to be essential. However, the floor seems to have little effect, since various arrangements of absorber over this area caused only minor changes in the field.

Some additional improvement in the field pattern was obtained by placing two vertical sections of absorber, in the form of a 90° "V" or "wedge", on the floor in front of the track and drive mechanism. This prevents radiation coming directly from the horn from reaching the metal parts of the track and being scattered to the probe. Room was left between the absorber and track so that when one of the diffracting objects was being studied, the base of the rod or prism support could also be placed behind the two sections of absorber. Fig. 5 and Plate 4 illustrate the placement of these two sections of absorber. Plate 4 also shows one section of absorber mounted on top of the 4 ft. high wall in front of the railing, and tilted back about 45°. This section is centered directly behind the probe, its purpose being to reduce reflection from the back wall. There is some reflection even from the hair absorber, and by placing one section of absorber in this way, some of the reflected energy is directed up, away from the probe. Two different colours of absorber can be seen in the photograph. They are essentially the same, the white absorber being a newer type. Plate 3 shows the transmitting or "Horn" end of the darkroom, the klystron and associated equipment being behind the end wall.

PLATE 3: DARKROOM: TRANSMITTING END

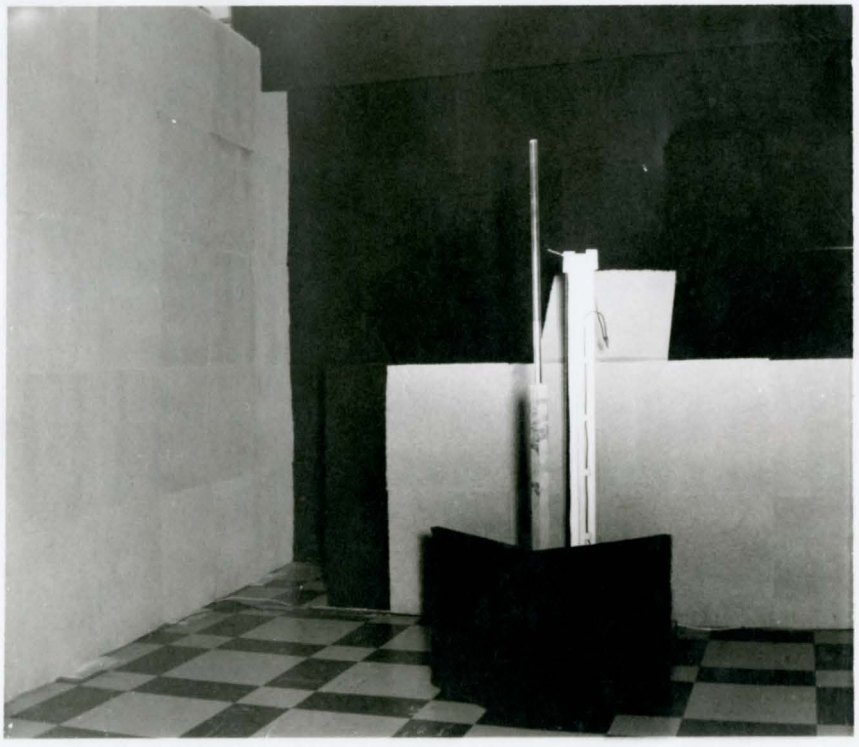

PLATE 4: DARKROOM: PROBE END

## 2-5 The Diffracting Cylinders and Prism

Five different cylinders are used in the diffraction experiment. Three of these are dielectric rods made of lucite, and two are conducting rods, one of brass, and one of foil-covered lucite. Two of the lucite cylinders are of circular cross section, one being 1 in. in diameter and 90 cm. long, and the other 1½ in. in diameter and 115 cm. long. The remaining dielectric rod is a 1½ in. semicylinder 95 cm. long, machined from a circular rod similar to the one mentioned above. The brass cylinder is a 1 in. outside diameter tube with a wall thickness of 1/32 in. and 200 cm. in length. The second conducting cylinder was made by coating the lucite semicylinder with a tight-fitting layer of aluminum foil. During the experiment, each cylinder, excluding the brass one, was held in place, at the lower end, by a wooden stand. The brass tube was fitted with an iron base of its own.

The prism, made by C. E. Jordan (7) in this laboratory, is a $45^\circ$-$45^\circ$-$90^\circ$ prism with two 33.3 cm. faces, a 46.9 cm. hypotenuse, and having a height of 50.5 cm. "Selectron 5026", a thermosetting plastic obtained from the Pittsburgh Plate Glass Co., was used in the construction.

# CHAPTER 3

## EXPERIMENTAL PROCEDURE AND RESULTS

### 3-1 Transmitter Stability

It is essential to an experiment of this kind that the amplitude and frequency of the incident radiation field be maintained constant to close tolerances. As indicated in section 2-1, means are available for monitoring the power level and frequency of the microwave energy in the wave guide leading to the horn. After an initial warm-up period of at least ten minutes, the power level was set to the desired value by the attenuator, and the reading on the monitor noted. During the course of the experiment, this level was constantly checked for any possible variation. It was found that the power level did not vary by more than 0.5% over a period of 2½ hours. An actual run took less than 20 minutes to complete, and the variation during this interval was negligible.

Although the klystron used was factory tuned to the working frequency of 9.375 kMc/sec., the actual frequency obtained depends to some extent on the tube voltages. The

tube may be operated in one of several different modes, and a small adjustment in reflector voltage is sufficient to bring the frequency to the desired value. However, in any given mode, the most stable operation was achieved by adjusting the voltages for maximum output. When ths was done (using "mode A"), the frequency was measured and found to be 9.380 kMc/sec., only 0.053% greater than the above value. All runs were taken with this setting.

In order to determine the stability of the frequency, the value was checked periodically. This had to be done immediately before or after a run, since tuning the frequency meter through resonance caused a small variation in the power level. It was found that after the initial adjustments, the frequency changed by less than 0.2% over a period of 2 hours. If the frequency drifted from the operating value by more than this amount, then the klystron voltages were readjusted for maximum power output.

## 3-2 Geometry of Diffraction Experiment and Placing of Rods

The axis convention used by Froese and Wait (3) has been adopted in this work, and is as follows. The geometrical axis of symmetry of the horn, or the axis of propagation, is called the x axis. The source of radiation, which is taken as the geometrical apex of the horn, lies directly on this axis. The y axis also lies in the horizontal plane cutting the x axis at the origin, which

locates the center of the cylinder. The axis of the cylinder is coaxial with the z axis, which runs vertically. (See Fig. 20).

In order to locate the cylinders correctly, the x and y axes were laid out carefully with pencil lines on the floor. The y axis was placed at a distance of 5.0 meters from the E-plane vertex of the horn. The exact position of this point over the floor was located by the use of a plumb bob. When one of the circular cylinders was to be placed in position, the front edge of the probe was moved to an x coordinate equal to the radius of the cylinder. To make this adjustment, the cylinder radius a was measured off on the positive x axis on the floor (in the direction away from the horn) and the front edge of the probe diode set over this spot with the plumb bob. The cylinder was then centered in front of the probe, barely touching it.

The semicylinders were more difficult to set up than the circular ones. The method used was to extend the y axis on the floor to the right hand wall, and to place a small mark on the wall directly above the axis. To arrange the cylinder to have its plane face away from the source, the probe edge was placed directly over the origin of coordinates, and the rod centered in front of the probe with its plane face just touching it. The cylinder was then rotated until the plane face lined up visually with the spot on the wall. To set the rod with its plane face toward the source, the probe edge was set behind the origin

by an amount equal to the radius of curvature a of the semicylinder. The curved face was then brought adjacent to the probe, and the plane face lined up visually with the spot on the wall.

The prism was placed in position in much the same manner as were the semicylinders. In both orientations of the prism the probe edge was first set directly at the origin. To set the prism up with its hypotenuse face away from the source, a fine pencil line was first drawn vertically down the center of this face. This facilitated the centering of the prism in front of the probe. The same spot on the wall was then used to line the hypotenuse up with the y axis. For the remaining case, a second spot was placed on the wall to the "horn" side of the first spot by a distance equal to the altitude of the triangular cross section of the prism. After the apex edge of the prism had been centered behind the probe, the hypotenuse face was aligned visually with this second marker. The exact positioning of each diffracting object is clearly indicated on the relevant figure. In all cases, except the two involving the prism, the objects are drawn to scale.

## 3-3 Procedure in Taking Runs

As explained in section 3-2, preliminary to setting any object in place, the probe had to be properly positioned at the origin, or behind it. Once this had been done for

either case, the meter stick on the optical bench was moved toward the horn until the nearest wire just made contact with the wheel on the trolley. This position was determined by listening for the click of the relays. After the correct position of the meter stick had been located, successive adjustments of the probe were made by means of the calibrating system rather than by the plumb bob.

Each of the experimental curves shown in Figs. 7-10, 13, 15, 16, 18, 19 is the result of averaging three independent runs on the corresponding object. Each run was preceeded by, and followed by a run on the incident field. The field runs before and after were compared to see that no noticable changes in the field pattern had occurred during the main run. The procedure was as follows. A field run was taken. The rod or prism was then set in place and a second run made. The object was then removed, and the field run repeated. This was followed by a second run on the object and so on, alternating field runs and diffraction runs. Thus each field run, except the first and last, served as both a run following, and as a run preceding two succeeding main diffraction runs. In analysing the results, the field run immediately following the diffraction run in question was used.

## 3-4 Analysis of Results

Since the units of intensity on the recorder chart

are completely arbitrary, and since the incident field itself does not comply to the ideal plane wave case, the intensity pattern of each diffraction run was normalized to the field pattern. Unfortunately, all reflections from the back wall could not be eliminated, and interference between the incident and reflected fields gave rise to a standing wave pattern along the axis of propagation. The pattern was found to be quite regular with a half wavelength spacing between adjacent peaks. A sample of the axial field patterns obtained is shown in Fig. 6. Since the standing wave pattern was regular and consistent, an average field value was used in obtaining the final results. The estimated average of the sample pattern is also shown in Fig. 6. The standing wave pattern superimposed on each main diffraction run was averaged out in a similar manner.

Because of the differentiator in the calibration circuit, no marker pip was produced corresponding to the surface of the object, and this had to be located on the chart by measuring back from the first marker the equivalent of 5 cm. of probe motion. By chance, the track and chart speeds are related in such a way that half an inch on the chart corresponds to one centimeter on the track. Points were taken not more than $\frac{1}{2}$ inch apart on the diffraction patterns, and normalized to the incident field value at the corresponding points. The three sets of results for each object were obtained separately, and the data for

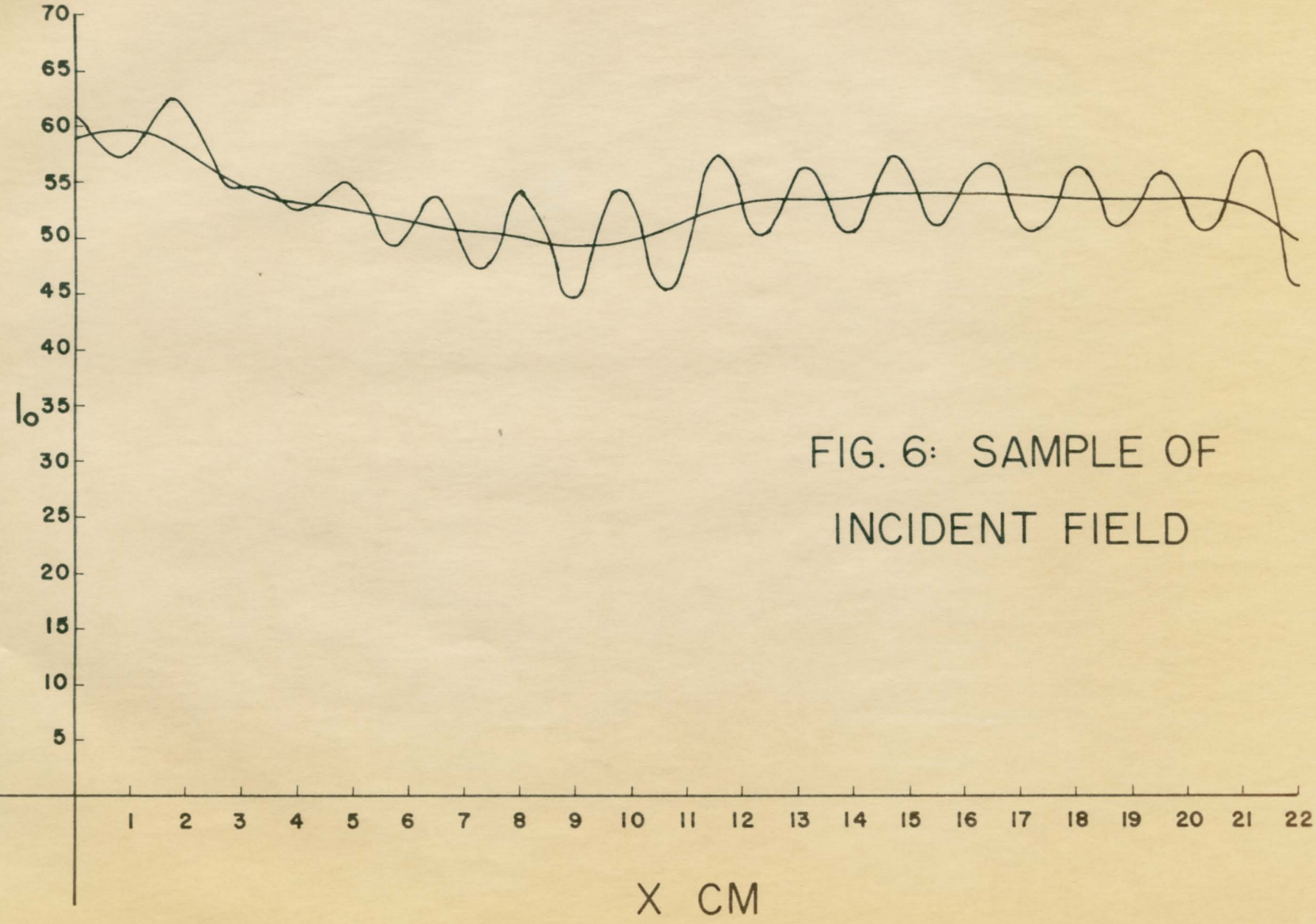


FIG. 6: SAMPLE OF INCIDENT FIELD

corresponding points averaged. The final averaged results are plotted in Figs. 7-10, 13, 15, 16, 18, 19 as stated earlier. In placing the points on the curves, the radius of the probe itself was also taken into consideration.

## 3-5 The 1 Inch Brass Rod

The observed diffraction pattern for the 1 inch diameter brass rod is shown in Fig. 7 along with the results of theoretical calculations. The calculated values were obtained using a formula derived by Froese and Wait (3), and are presented as the dash-dot curve in the figure. This formula is given in the Appendix along with a brief description of the procedure used in the calculations.

As expected by theory, the intensity very near the surface is small, approaching zero. The actual intensity right at the surface could not be observed because the distance of closest approach of the probe axis to the cylinder was determined by the probe radius, 0.125 cm. The experimental curve is very similar in shape to the theoretical one, but is noticably higher, particularly in the region close to the cylinder. The finite length of the probe is likely responsible for this effect. Ideally, the probe should be of zero length, since it is placed normal to the axis of symmetry of the cylinder. The ends of the diode extend beyond the x axis a distance of 0.35 cm., or $\frac{1}{4}$ of the cylinder radius a. Hence, when the probe

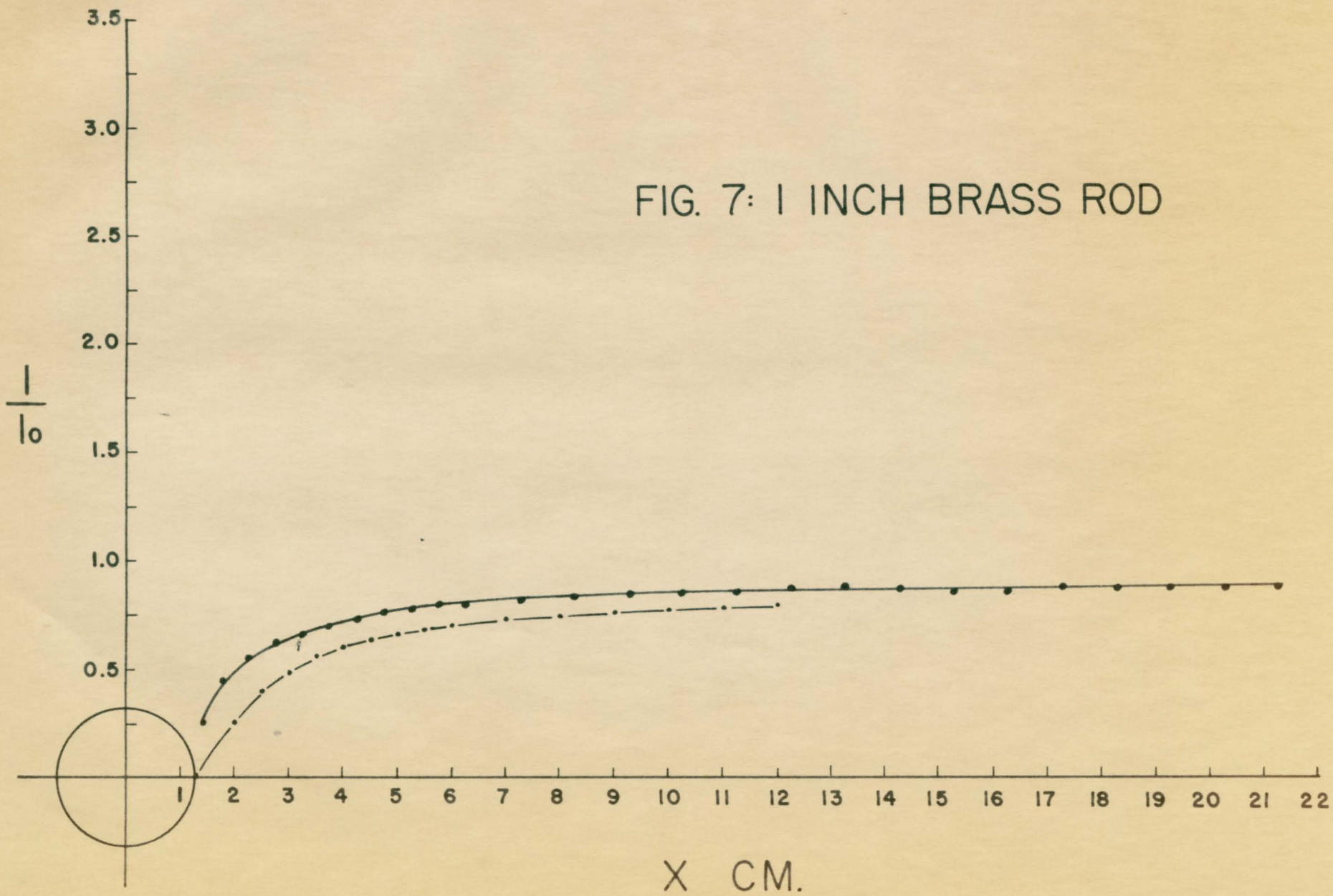


FIG. 7: 1 INCH BRASS ROD

is immediately behind the rod, the extremities of the diode extend beyond the axis into regions where the field intensity is noticably different from zero. The observed field intensity is thus higher than it should be according to the theory.

The experimental curve rises sharply within the first wavelength from the surface, reaching 80 per cent of its final value in this region. As well as being higher than the theoretical curve, the experimental one also rises more steeply near the cylinder. Beyond this region, the field intensity approaches the value it would have if the cylinder were not present. It is clear from the figure that the finite length of the probe is not such an important factor well back from the surface.

## 3-6 The 1½ Inch Foil-Covered Semicylinders

The diffraction patterns of the two aluminum-coated semicylinders are quite similar to that produced by the full brass cylinder. The most significant difference is the field value o.125 cm. from the surface. When the plane face was set looking away from the source, the intensity very close to the cylinder was found to be almost zero (Fig. 8). The distance across the plane face is 1½ inches, appreciably greater than the length of the diode. Also, unlike the case of a circular conductor, the plane face of the semicylinder does not curve away from the probe leaving parts of it a significant distance from the rod.

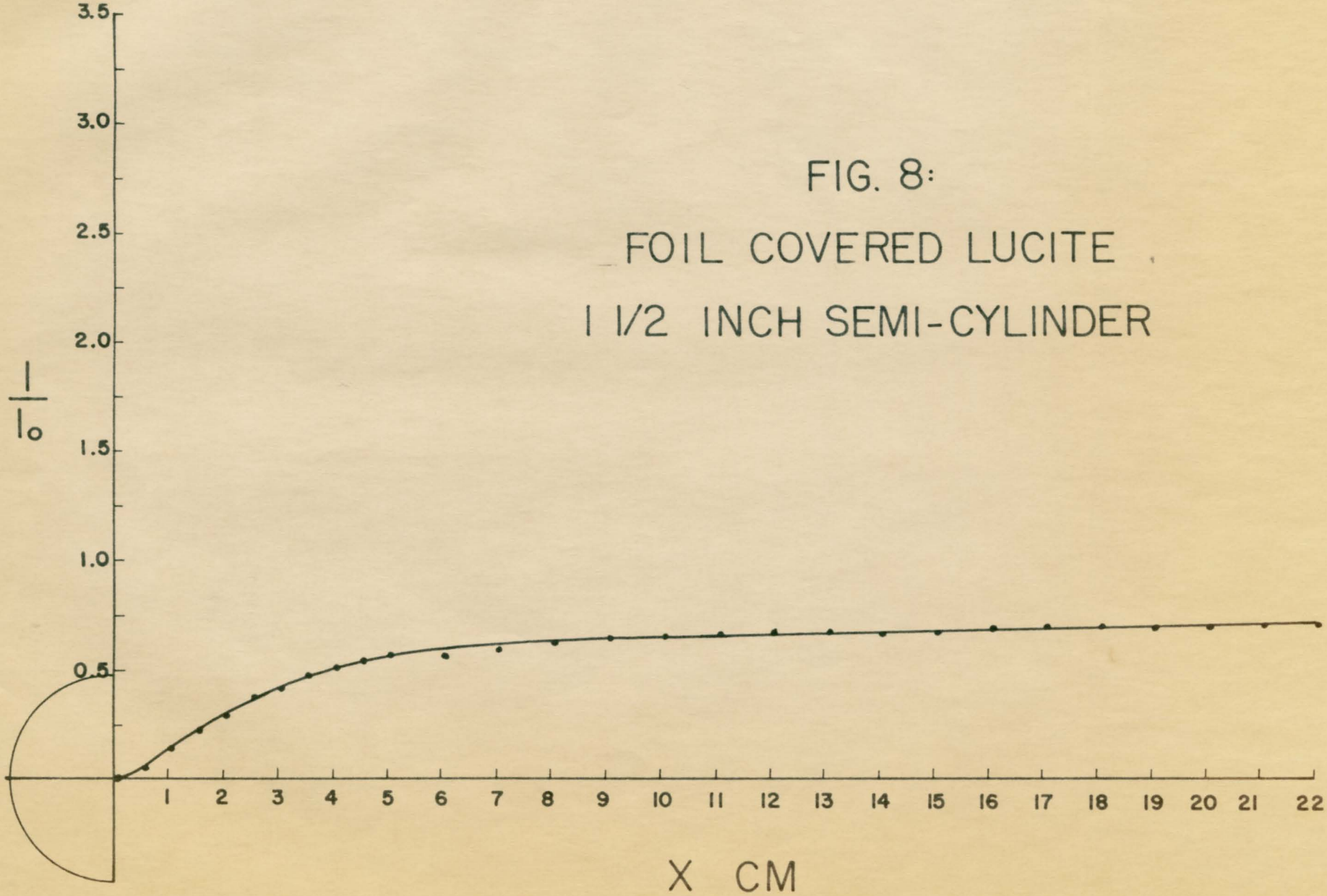


FIG. 8:

FOIL COVERED LUCITE

1 1/2 INCH SEMI-CYLINDER

The initial slope is not as great as for the 1 inch brass tube, and the curve levels off at a lower value. However, the long gradual rise which takes place beyond about three wavelengths of the surface has a slope nearly twice as great.

The case with the plane face toward the source is shown in Fig. 9. As with the brass rod, the field behind the curved face is not zero, although it is much closer to it. Both the probe length and the probe diameter become less important as the size of the rod is increased. Similar to the circular cylinder case, the intensity rises more rapidly behind the rod than it does for the preceding semicylinder case. The only noticable difference in the patterns for the two semicylinders occurs within about $1\frac{1}{2}\lambda$ from the surface, the two intensities becoming almost identical beyond this region.

## 3-7 The 1 Inch Lucite Circular Cylinder

Fig. 10 shows the experimental and theoretical curves for the 1 inch lucite rod. (Actual measurement showed the rod to have an average radius of 1.233 cm. at the center.) Experimentally, the intensity rises sharply and continuously as the surface of the cylinder is approached. Theoretically, however, there is an intensity maximum about $0.12\lambda$ from the surface. That this is not observed is most likely a

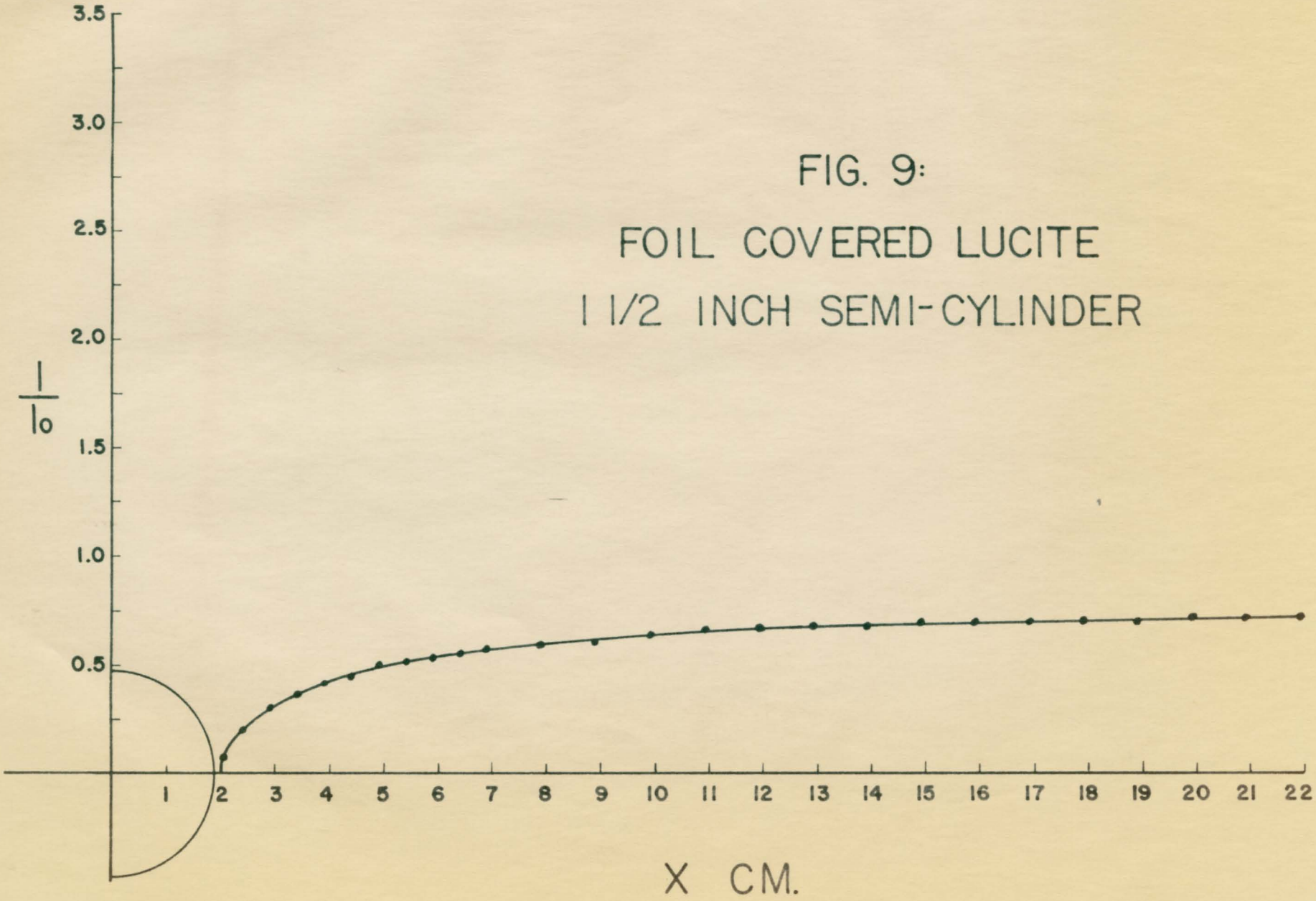
FIG. 9:
FOIL COVERED LUCITE
1 1/2 INCH SEMI-CYLINDER
3.5
3.0
2.5
2.0
1.5
1.0
0.5
I/Io
1
2
3
4
5
6
7
8
9
10
11
12
13
14
15
16
17
18
19
20
21
22
X CM.

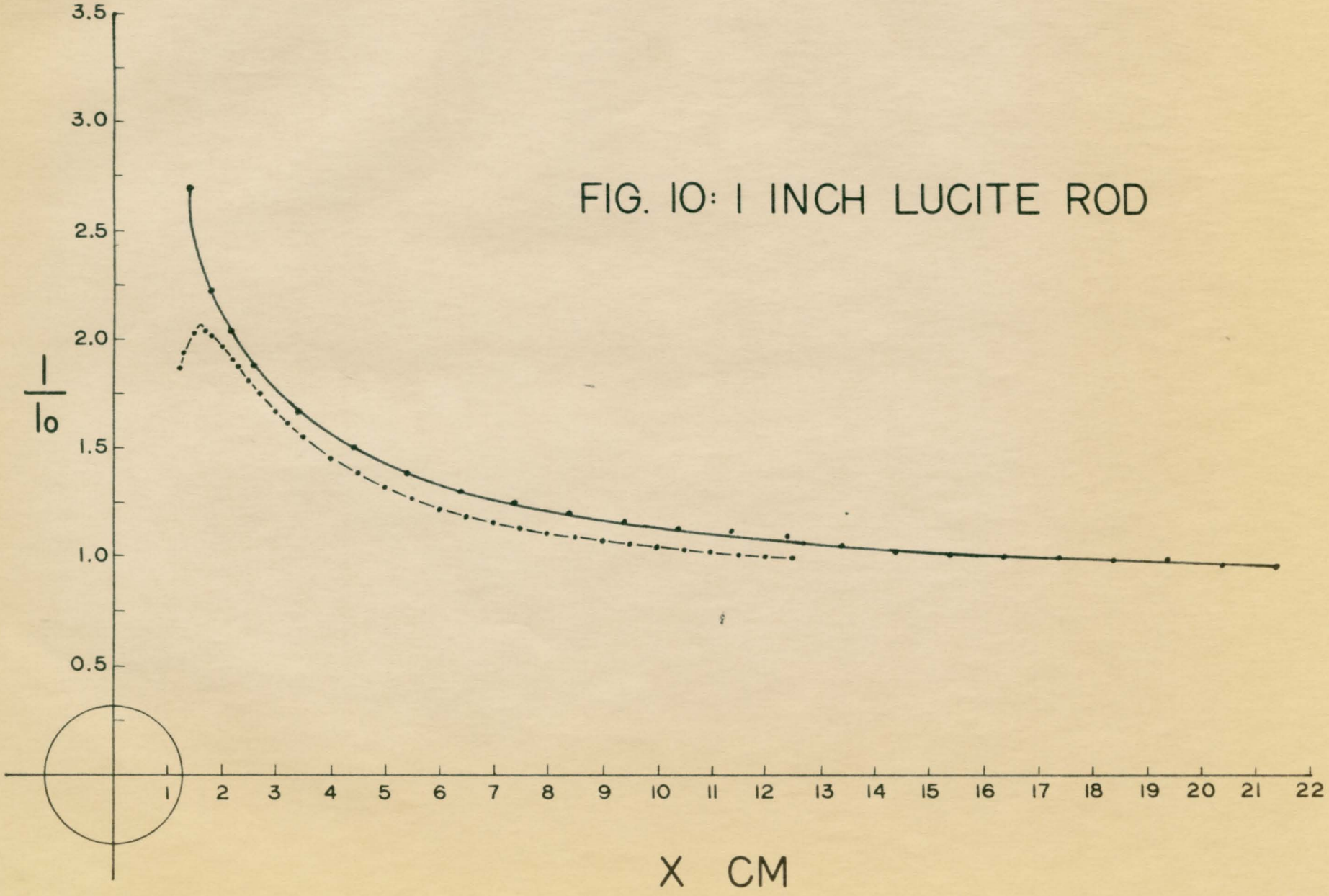


FIG. 10: 1 INCH LUCITE ROD

result of the integration of intensity over the finite length of the probe diode. Reradiation from the probe to the cylinder and back to the probe again, is an experimental disturbance which may also modify the ideal field pattern at closest approach.

According to geometrical optics, there is a partial focussing of the radiation in a cusp shaped region immediately behind the rod as shown in Fig. 11, and discussed in some detail in Ref. 4. There does not exist any sharply defined focal line through which all the radiation passes. Rays which passed through the cylinder making small angles with the x axis form the tip of the cusp. Incident rays 2, 3, 4, and 7 in Fig. 11 are equally spaced, so that the flux contained between adjacent rays is the same in each case. It can then be seen that, after passing through the cylinder, the flux density on the x axis is greatest in the region near ray 2. In addition to the greater density of rays cutting the x axis in this region, the smaller initial angles of incidence of these rays on the cylinder results in a greater fraction of the energy being transmitted than for rays incident more obliquely. Closer to the surface of the cylinder, the density of rays near a given point on the axis is less, in accordance with the theoretical results.

Because of the physical size of the detector, rays off the x axis contribute to the observed field intensity as well as do the desired ones on the axis. Consequently, as

# FIG. 11: REFRACTION OF RAYS BY LUCITE ROD

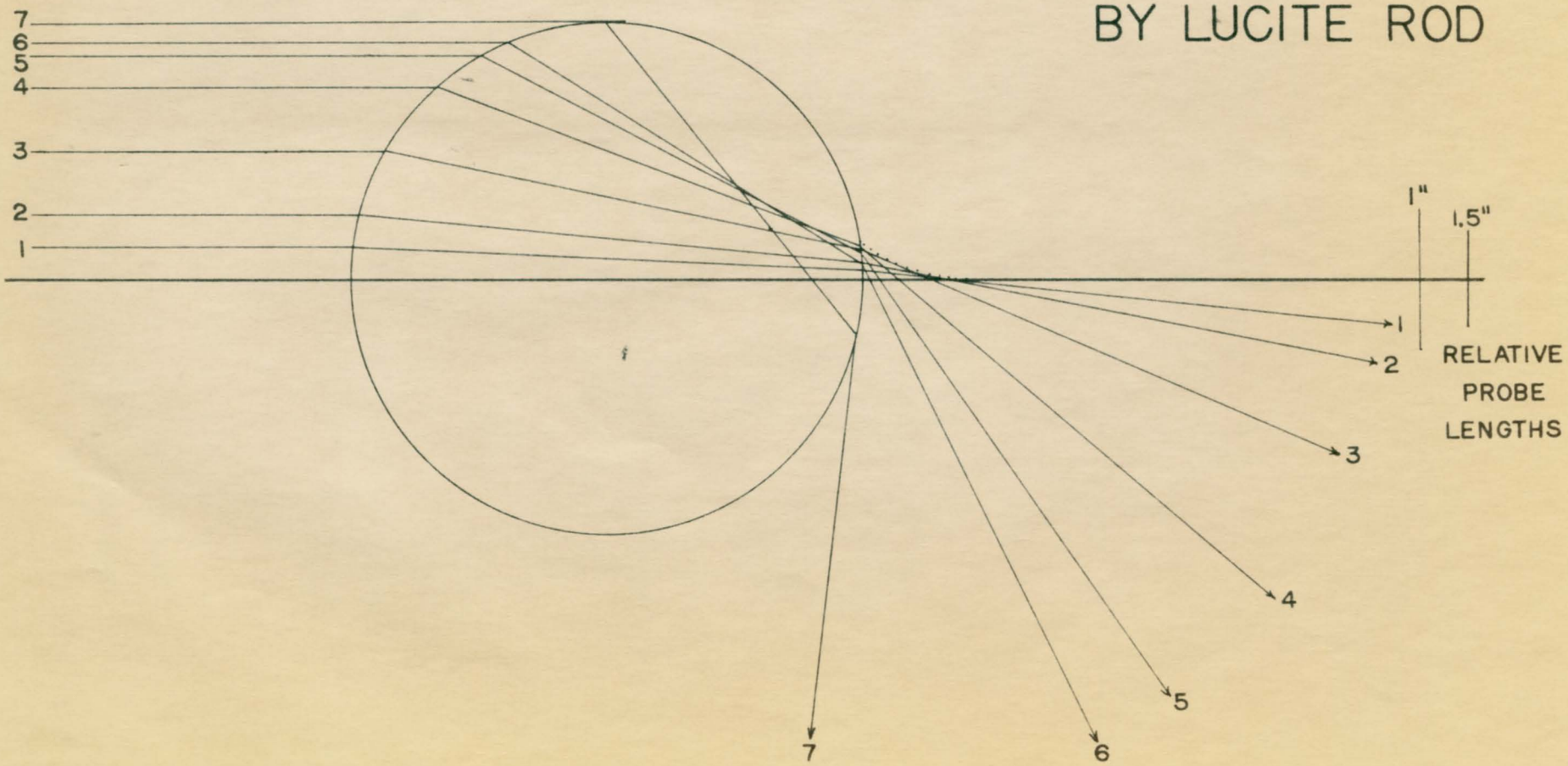

the probe is moved from the tip of the cusp-shaped region toward the cylinder, a larger number of rays are intercepted by it. In addition, the probe is more sensitive at the ends than it is at the center. While the intensity on the axis decreases, the total energy extracted from the field appears to increase. This is equivalent to saying that the intensity integrated over the length of the probe increases even though the intensity on the axis alone decreases. In order for this to occur, the width of the peak spanned by the probe would have to increase as explained below.

The field pattern along a line parallel to the y axis and at various distances behind the cylinder exhibits a high peak on the x axis. On either side of the x axis, the intensity drops off rapidly becoming nearly zero within 1 or 2 cm. With the probe placed parallel to the y axis as in this experiment, only a small section near the center of the diode experiences the full field intensity representative of the peak value on the x axis. The ends of the diode extend beyond the peak into regions where the intensity is lower. Hence, the measured value of the field, which is the result of the integration of intensity along the length of the probe, should be lower than the actual value on the x axis. And, for the observed field intensity to increase while the peak value actually decreases, the peak would have to become wider in such a way that the increased effect at the ends of the diode outweighs the

reduced effect at the center.

Unfortunately there are no experimental results available to verify this hypothesis. Any attempt to determine the actual shape of the peak behind the rod would suffer the same difficulties of resolution as the present experiment. Results obtained by Subbarao and McLay (ref. 4) using the parallel polarization do not show any evidence of either the broadening of the peak, or the lowering of the peak on the x axis as the rod is approached. However, the 1N23A probe diode used in this previous work had a radius of about 0.27 cm., and the effect under consideration occurs in the theoretical curve at distances less than 0.4 cm. from the surface of the rod. This distance is not significantly different than the radius of the probe itself, and a further investigation in this region using a probe of smaller diameter may prove profitable.

The field intensity behind the rod drops sharply within the first wavelength or so from the surface as expected from geometrical optics considerations. However, contrary to the previous discussion, it always remains above the theoretical curve. It is seen that simple geometrical optics is inadequate to explain fully the experimental results. A more rigorous treatment would include the diffraction around the rod, which has not been taken into account in the above geometrical optics treatment. However, all such effects are included in the solution of the theoretical field equations. There is thus no explanation immediately available

for the fact that the experimental curve is above the theoretical one in this case.

The theoretical determination of the diffraction pattern along the x axis was continued for points inside the cylinder itself. The results of these calculations are shown in Fig. 12 along with the points already presented in Fig. 10. A few points outside the cylinder in the negative x direction were also determined to show the continuity of the curve at the surface.

It is seen that there are two peaks of intensity inside the rod each of which is narrower than the one outside at x=1.6 cm. The peaks (and the troughs) become lower as x decreases algebraically.

## 3-8 The 1½ Inch Lucite Circular Cylinder

The 1½ inch lucite rod (fig. 13) produces an observed diffraction pattern similar in form to that of the 1 inch rod, but with a 13 per cent higher peak. The most outstanding difference between the two cases is the fact that the intensity behind the 1½ inch rod drops to a much lower value. At a distance of about 3 wavelengths from the surface of each cylinder, where the two curves have nearly levelled out, the intensities differ by a factor of more than 5. However, the tail end of the experimental curve in fig. 13 shows a very slight upward slope suggesting that the value rises again many wavelengths from the cylinder. The curve for the 1 inch rod, in contrast, is ~~still falling~~

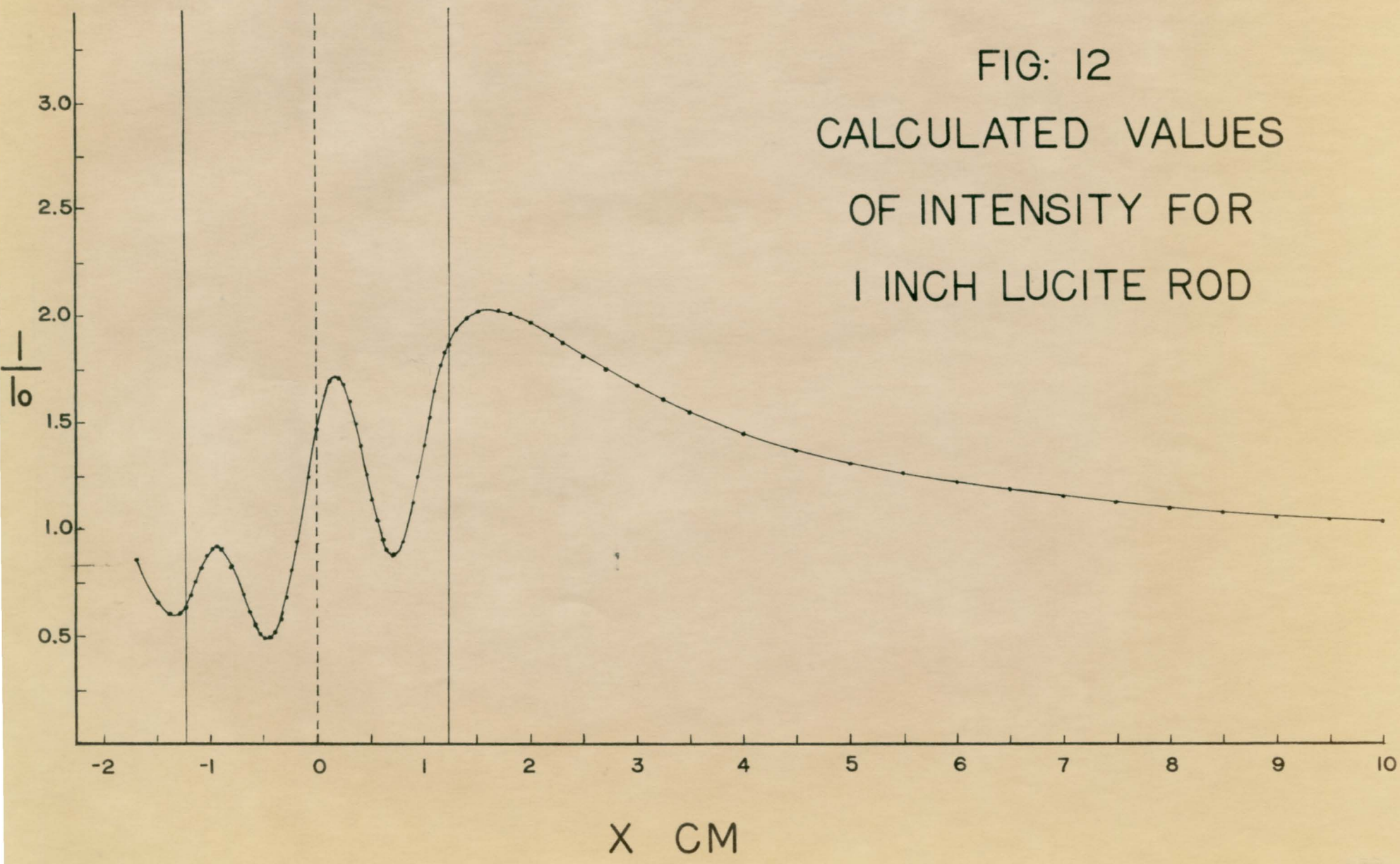
FIG: 12
CALCULATED VALUES
OF INTENSITY FOR
1 INCH LUCITE ROD
I/Io
3.0
2.5
2.0
1.5
1.0
0.5
-2
-1
0
1
2
3
4
5
6
7
8
9
10
X CM

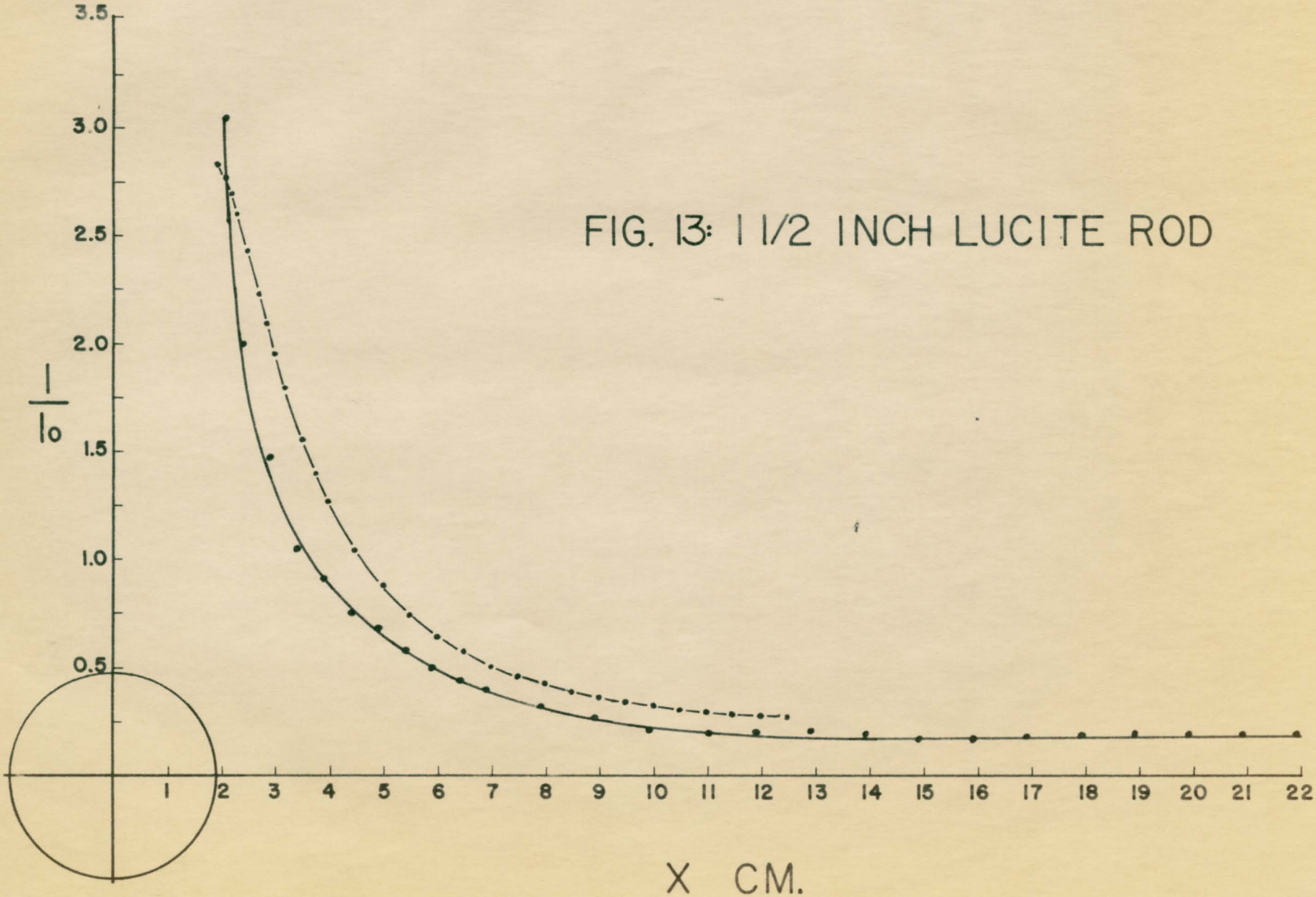


FIG. 13: 1 1/2 INCH LUCITE ROD

still falling in this same region.

The theoretical results for the 1½ inch rod (measured radius 1.916 cm.) differ from those of the 1 inch rod in two outstanding ways. There is no large peak of intensity outside the cylinder on the positive x axis as in the 1 inch case. Also, the theoretical curve lies almost entirely above the experimental one, as expected from previous general considerations. Only at points very near the surface is this situation reversed. Beyond about 6 or 7 cm. from the surface of the rod, the two curves become very nearly parallel.

As was done for the 1 inch lucite rod, points were calculated for x values inside the cylinder. Fig. 14 shows the results of these calculations. There is a sharp peak of intensity very close to the surface with the value inside dropping quickly to a minimum of less than half the surface value. There are three peaks of intensity lying entirely inside the rod, and these have rapidly decreasing amplitude with decreasing x as in the previous case. The four peaks, including the one at the surface, are nearly equally spaced, having a separation of 1 cm. This is just a half wavelength for the 10 KMc/sec. radiation when traversing a dielectric of refractive index n = 1.6.

## 3-9 The 1½ Inch Lucite Semicylinder

The two cases of the lucite semicylinder, shown

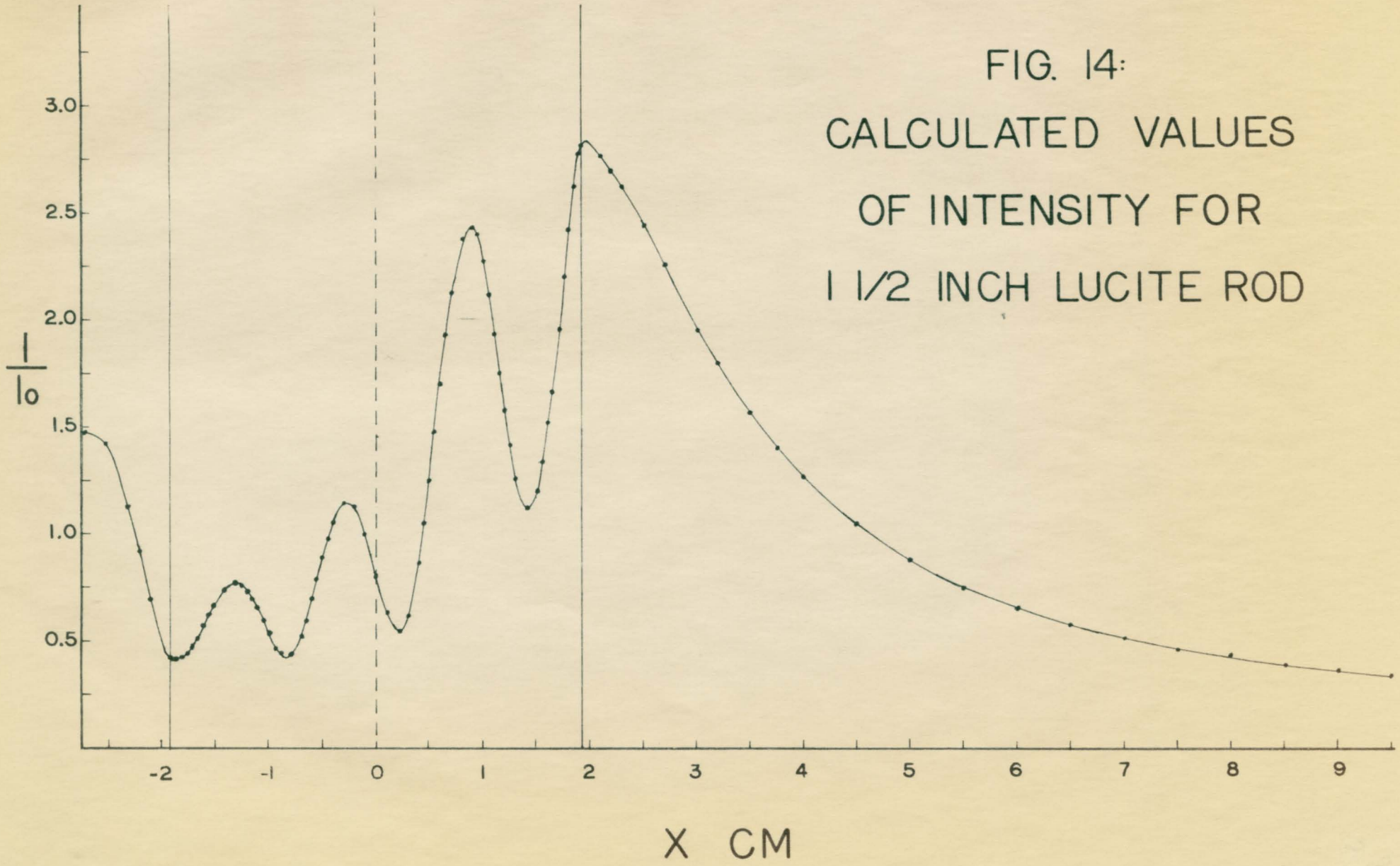


FIG. 14:
CALCULATED VALUES
OF INTENSITY FOR
1 1/2 INCH LUCITE ROD

in Figs. 15 and 16, are seen to be very similar in form. Both curves rise to a peak about 2 cm. behind the back surface of the rod. The heights of the two peaks are nearly the same, with that shown in Fig. 15 being roughly 3% higher than that in Fig. 16. These peaks indicate that there is a partial focussing of the radiation behind the cylinder in each case. There is, as with the full lucite cylinders, a caustic region behind the rod where the intensity is large, falling off with increasing x.

As shown in Ref. 5 and Fig. 17, the caustic region behind the two semicylinders is larger and extends further "along the x axis" than it does in the case of the full cylinders. In addition, the intensity should not decrease as rapidly with increasing x for this case. Inspection of Figs. 13, 15 and 16 shows this prediction to be in agreement with experiment.

## 3-10 The Dielectric Prism

The diffraction patterns for the selectron prism are shown in Figs. 18 and 19. In the first case (Fig. 18) several high peaks are observed along the x axis, the distance between peaks increasing with increasing x. As shown in Ref. 9 for a similar orientation of the dielectric prism, the incident beam is split by the prism into two overlapping beams. There is strong interference of the two beams in the region of overlap, producing a set of interference

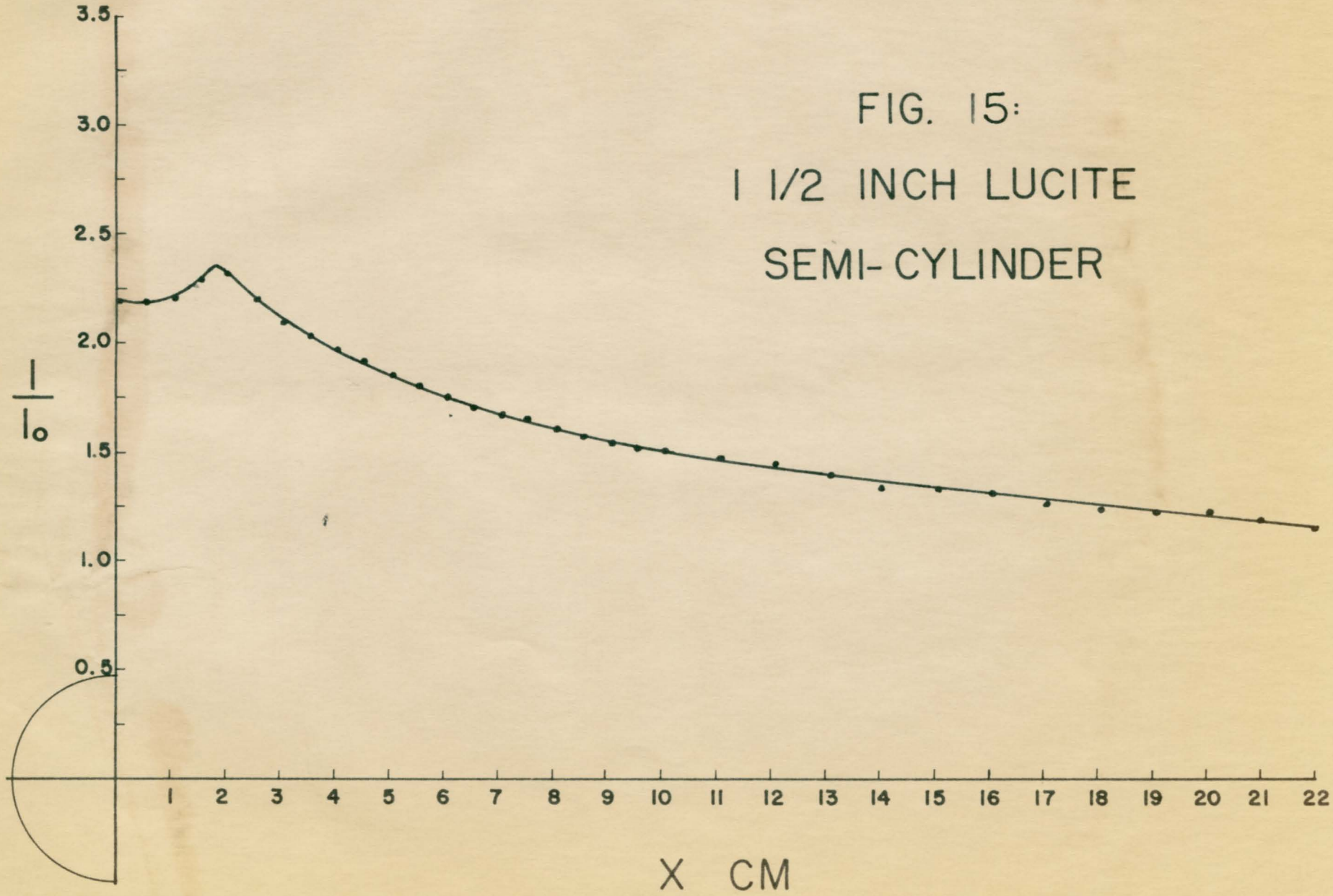


FIG. 15:

1 1/2 INCH LUCITE

SEMI-CYLINDER

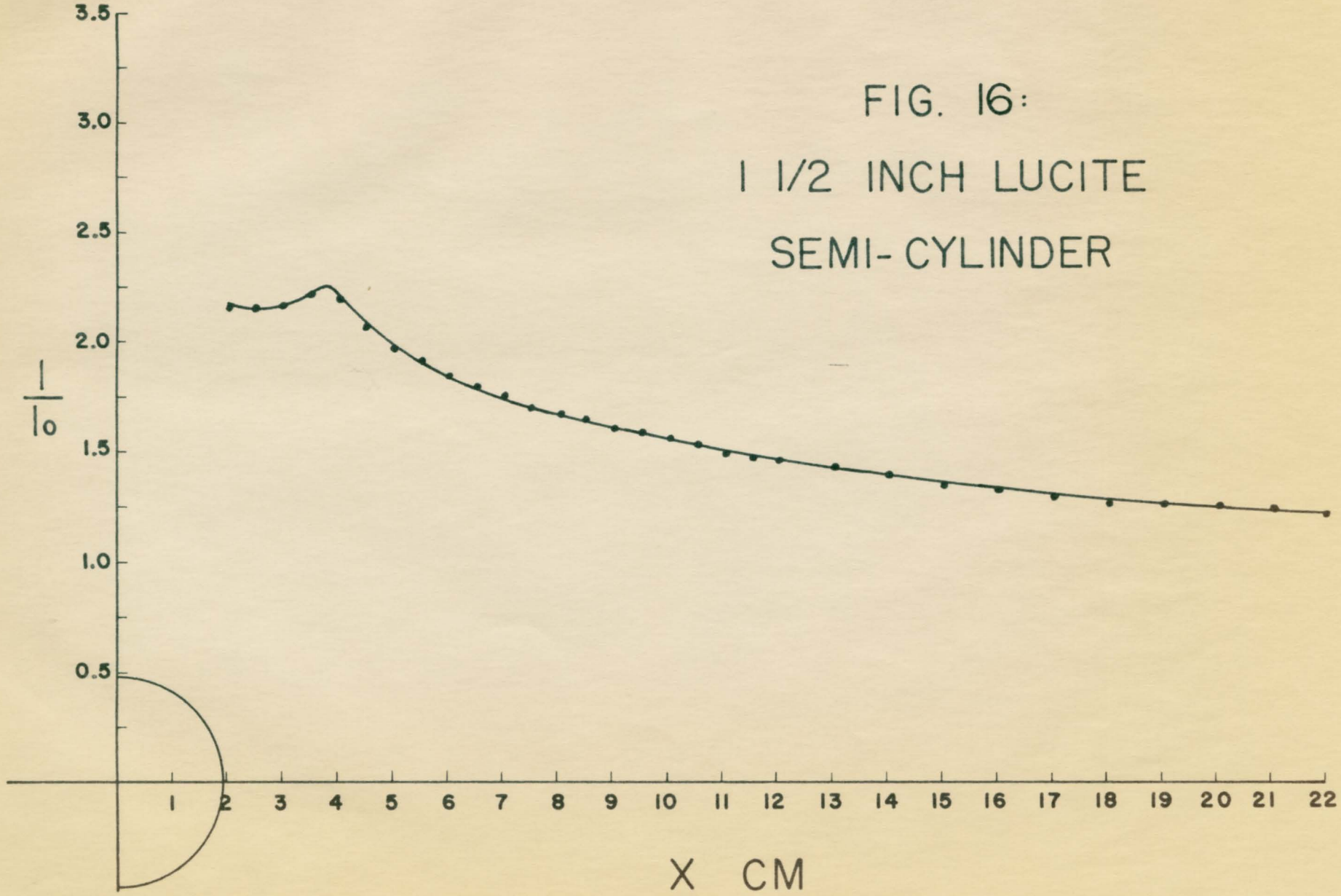


FIG. 16:

1 1/2 INCH LUCITE

SEMI-CYLINDER

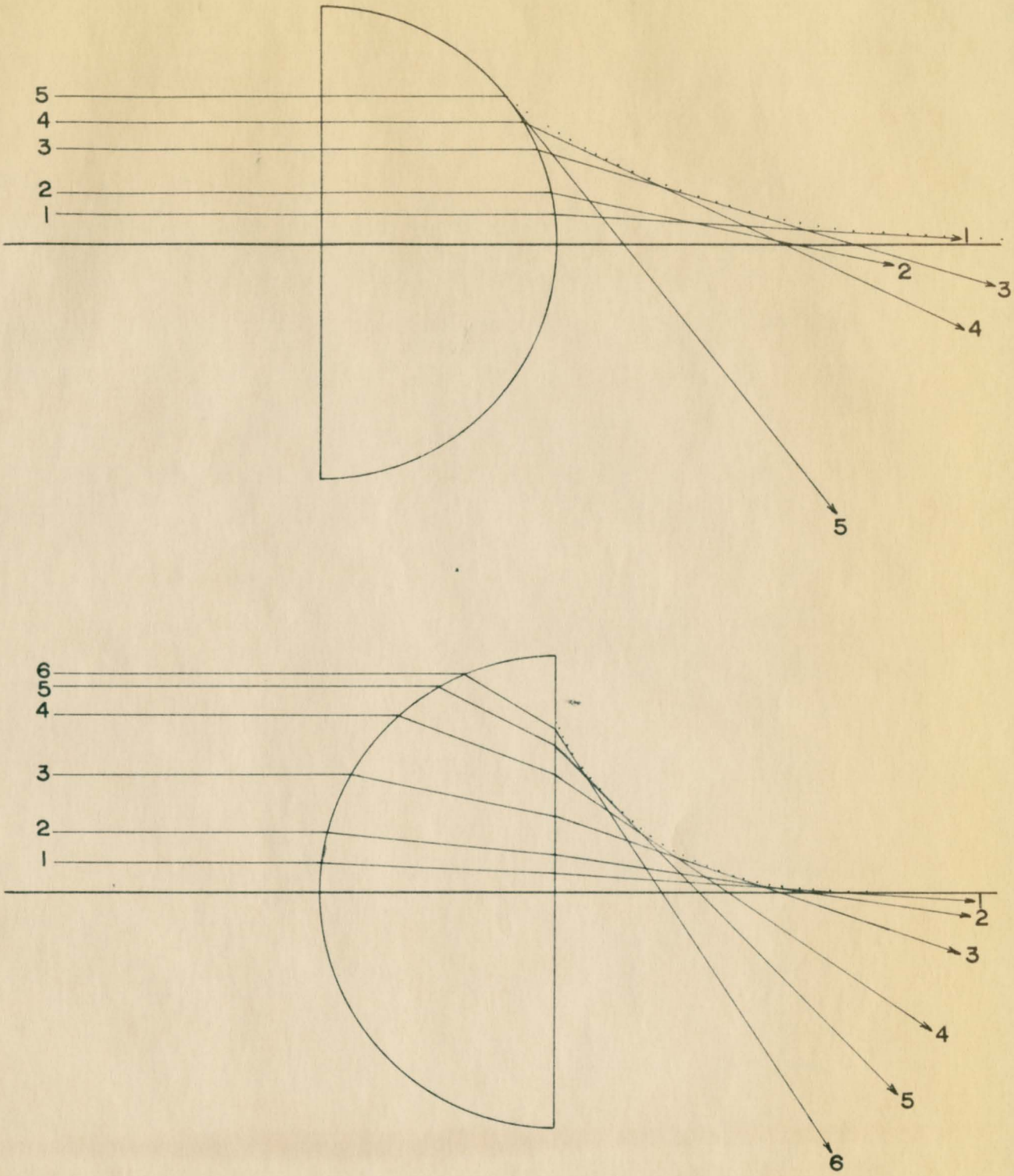


FIG. 17: REFRACTION OF RAYS BY LUCITE SEMICYLINDER

fringes along any horizontal line normal to the x axis. Along the x axis itself, however, there should be no significant intensity variation as a result of interference alone. This follows from the fact that corresponding rays in the two overlapping beams travel equal optical path lengths to reach a given point on the axis. Each beam has, however, effectively passed through a diffracting aperture approximately 10 wavelengths wide, and will thus have a diffraction pattern superimposed on it. The superposition of the two beams, and hence of their corresponding diffraction patterns, will result in a variation of intensity along the x axis. It is likely that the pattern observed can be explained in terms of this superposition of diffraction patterns.

It is readily shown that the two beams from the "biprism" overlap out to a distance of about 33 cm. on the x axis (see Ref. 9, Fig. 6). Beyond this point the intensity would be expected to fall off smoothly with increasing x. Such is seen to be the case, at least within the region in which observations were made.

The second case of the prism, with the hypotenuse face toward the source (Fig. 19), is very dissimilar to the case just considered. There is total internal reflection of rays from the two oblique faces so that, according to geometrical optics, all radiation incident on the hypotenuse face is eventually returned along the path of the incident

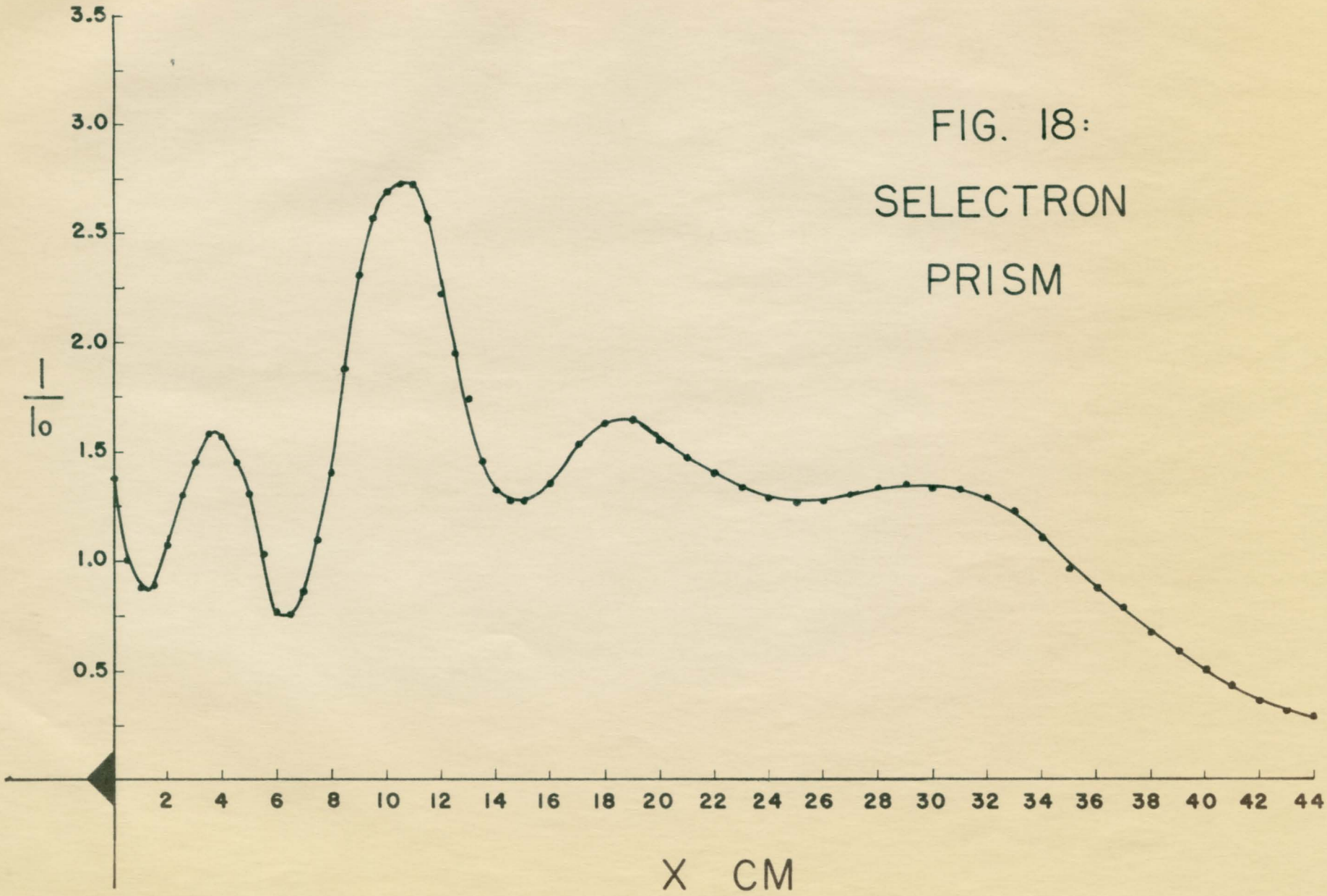


FIG. 18:
SELECTRON
PRISM

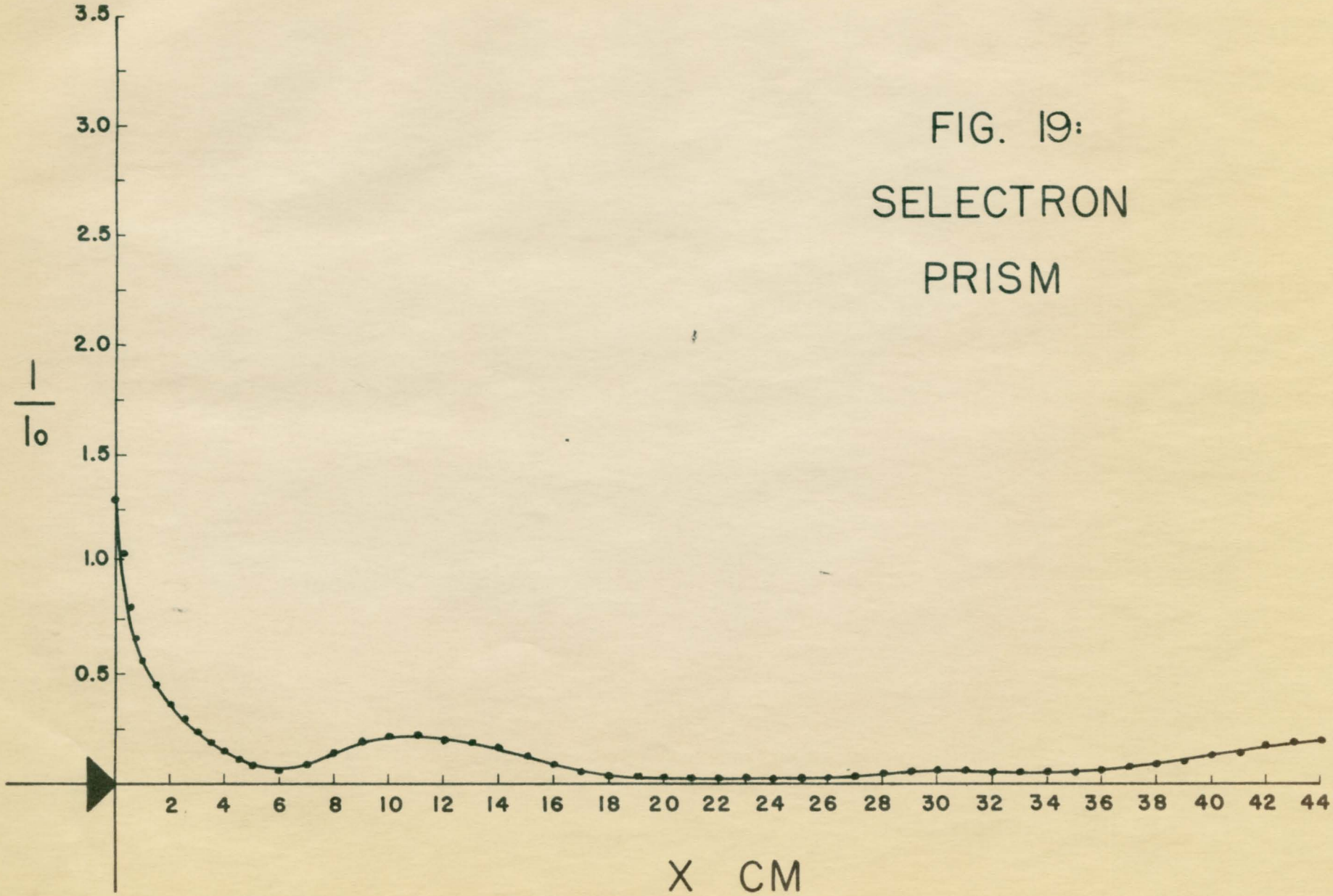


FIG. 19:
SELECTRON
PRISM

beam. In this ideal case, the intensity behind the prism anywhere within its geometrical shadow would be zero. In reality, the observed intensity behind the prism is finite but much lower than that observed in the previous case. Only very close to the apex edge of the prism is the intensity appreciable. According to electromagnetic theory, there is an evanescent wave propagated parallel to the plane dielectric surface of the prism in the optically less dense medium when the angle of incidence of radiation on the surface from the optically dense side equals or exceeds the critical angle. The amplitude of this disturbance decreases exponentially with increasing distance from the surface. There is, in addition, no net energy flow through the surface unless the evanescent wave is disturbed by the presence of an object such as the diode probe. As seen in Fig. 19, the evanescent waves propagated behind the two totally reflecting faces of the prism appear to merge and reinforce in the region close behind the 90° corner. The same effect was observed near the 90° apex edge of the prism by Hedgecock using a polarization parallel to the edge (see Ref. 9, Fig. 8).

## 3-11 Effect of Probe Orientation on Observed Patterns

The comparison between theory and experiment for the three circular rods shows that there is, in each case, a discrepancy between the calculated and observed results. An attempt was made to explain this fact in terms of the

finite length of the probe diode. After the results presented in this thesis had been obtained, a defect in regard to symmetry of the probe was discovered. Tests were being conducted to determine the feasibility of reducing the effective length of the diode in the horizontal plane by rotating it about the axis of the support rod until it made a small angle with the (vertical) z axis. In this way, only a small component of the horizontally polarized field would be detected. The amplifier gain was increased to allow for the decreased sensitivity of the probe, when in this position, to the horizontal electric vector of the incident field. The field pattern observed with the probe in this orientation was identical to that with the probe horizontal, as long as a diffracting object was not in place. When runs were made with a cylinder in place, the results obtained did not agree with previous results except as regards the general form of the curve.

As a result of this particular investigation, it was found that the normalized field intensity patterns behind the diffracting rods are in some way dependent on the angle between the probe axis and the z axis. In addition to this, the results for angles 180° apart were not identical with those obtained by turning the diode end for end (180° rotation). However, in this special case, the difference is relatively small.

No explanation of this effect is forthcoming as

yet, although the physical construction of the diode itself appears to be partly responsible. Other probes constructed from different diodes of the same type gave the same results, even when the diode mounting was modified. It is possible that the pattern of response of the diode to radiation coming from different directions is not symmetrical about the center of the diode. (This possibility was mentioned in section 1-3 in connection with field measurements made off the x axis.) This could result from the geometrical asymmetry of the crystal and "cat's whisker" in the diode construction. In this case, different intensities of radiation reflected from the walls, and incident on the probe from different directions, could modify the observed patterns in a way depending on the orientation of the diode in the field.

Reflection of radiation from the walls of the darkroom may give rise to small electric field components in the z direction. The angle between the z axis and the probe axis will determine the extent of response of the probe to this z component if present. Some spurious response of the probe to the x component of this field can also be expected partly as a result of misalignment of the probe parallel to the yz plane. Even if perfect alignment of the probe axis were possible, all parts of the "S" shaped "cat's whisker" do not lie along this axis and will be sensitive to other field components. However, on the positive x axis the x component arising as a result of the interaction

of the incident field with the cylinder will be very small, reflections from the walls providing the main contribution.

## 3-12 Conclusions

The main objective of this experiment was the evaluation of the performance of the field measurement apparatus for the special case of polarization perpendicular to the plane of incidence. As stated earlier, diffraction measurements using this polarization present special difficulties in the design of the detecting probe. Of major concern is the physical size of the probe itself, particularly its length. The comparison between experimental and theoretical results indicate that, as suspected, a simple crystal diode probe is not very suitable for use in experiments with a polarization perpendicular to the axis of symmetry of the diffracting cylinders. The smallest microwave diodes presently available are still too large to give good results with the wavelengths and object sizes most convenient for experimental investigations.

In addition to this problem, the difficulties encountered, apparently as a result of symmetry defects, also indicate that special attention must be given to the design of probes for use with this polarization. The internal structure of the microwave diode itself appears to be at least partly responsible for the asymmetry of the directional characteristics of the probe, and probably gives rise to a spurious sensitivity to field components

normal to the probe axis. Other possibilities worthy of consideration for the construction of probes include thermal detectors such as bolometers or thermistors, simple electric dipoles made of wire, and magnetic field detectors (loop antennae).

In spite of the shortcomings of the probe, the main features of the diffraction patterns of the various rods and prism have been determined experimentally. In all cases involving cylinders, the intensity either decreases or increases smoothly with increasing x. As expected, the intensity behind conductors is small near the surface, increasing with increasing distance along the x axis. The opposite is the case for dielectric cylinders, at least for the shapes studied.

Calculations carried out for points inside the two lucite circular cylinders have produced interesting results which cannot be determined experimentally. The oscillating patterns inside the rods are quite different in structure from the patterns outside along the positive x axis. In each of the two cases, there is a high peak of intensity inside the dielectric cylinder between $x=0$ and $x=a$. Similar calculations for the two rods taking the polarization parallel to the axis of each cylinder, have just been completed by Dr. A. B. McLay. These results, which will not be presented here, are quite similar to those already presented except for one noticeable difference. $\lambda_c$

The intensity near the surface behind each cylinder was found to be much higher than in the present case (by a factor of more than 2). However, the height of the peaks inside the rods was seen to be much lower in each case. Thus, the value of $|E_z/E_o|^2$ in the "parallel" case is large at the surface ($x = a$) of the cylinder and small at the position of the peaks inside. The value of $|E_y/E_o|^2$ in the "perpendicular" case is relatively small at the surface, and relatively large at the position of the peaks inside the rods. Previous experimental measurements made by Dr. McLay and other workers in this laboratory, using the polarization parallel to the axes of the rods, agree fairly well with the high intensity values calculated for this case near the surface of the cylinder. A check on the calculations in both cases is afforded by the continuity of the calculated curve through each surface.

## APPENDIX

## THE THEORETICAL FIELD EQUATIONS

In studies of the diffraction of electromagnetic waves around objects comparable in size to the wavelength, only very crude explanations of the observed patterns are possible using simple geometrical optics. No simple physical argument is sufficient for a complete quantitative description. In such cases, a solution of Maxwell's equations with the proper boundary conditions is necessary for a satisfactory theoretical analysis.

Froese and Wait (Ref. 3) have solved the boundary value problem for a cylinder of infinite length, having dielectric constant $\epsilon$ and permeability $\mu$. The cylinder is surrounded by a medium with constants $(\epsilon_o, \mu_o)$. Fig. 20 shows the geometry of the diffraction experiment. For a dielectric rod and incident radiation polarized with electric vector perpendicular to the cylinder axis, the result is given as follows.

$$\frac{E_y}{E_o} = e^{i\phi_o} - \sum_{m=o}^{\infty} C_m \, i^m \, e^{-i\eta_m^*} \sin \eta_m^* \, F_m \qquad (1)$$

(For radiation emanating from a "line" source at (-x,0).)

where

$$\phi_o \simeq k\left[\sqrt{(x+x_o)^2+y^2} - x_o\right]$$

$$k=\frac{2\pi}{\lambda} \qquad \lambda = \text{free space wavelength.}$$

$$C_o = 1, \quad C_m = 2 \quad (m \neq 0)$$

$$\phi = \tan^{-1}\frac{y}{x} \qquad N = \left(\frac{\epsilon_1}{\epsilon_o}\right)^{\frac{1}{2}}\left(\frac{\mu_1}{\mu_o}\right)^{\frac{1}{2}}$$

$$\tan \eta_m^* = \tan \delta_m(ka)\,\frac{N^2 \tan \alpha_m(ka) - \tan \alpha_m(Nka)}{N^2 \tan \beta_m(ka) - \tan \alpha_m(Nka)}$$

$$\tan \delta_m(x) = -\,J_m(x)/Y_m(x)$$
$$\tan \alpha_m(x) = -\,xJ_m'(x)/J_m(x)$$
$$\tan \beta_m(x) = -\,xY_m'(x)/Y_m(x)$$

and

$$F_m = \cos m\phi \cos\phi\, H_m^{(1)'}(k\rho) + \frac{m \sin m\phi \sin\phi\, H_m^{(1)}(k\rho)}{k\rho}$$

where

$$\rho = (x^2+y^2)^{\frac{1}{2}}$$

The result (1) is expressed as a ratio of the measured field to the incident field at the point (x,y), and gives the normalized electric field value.

For the cases of interest in this experiment, the coordinate y is zero, which results in a considerable simplification in the evaluation of some of the above expressions. With this condition imposed, we have, for points outside the cylinder,

$$\phi_o \simeq kx \quad \text{(x may have positive or negative values)}$$

$\phi = 0$ (for positive x), or $\pi$ (for negative x)

$\rho = |x|$

$F_m = H_m^{(1)'}(k\rho)(\cos m\phi \cos \phi)$

so that (1) becomes

$$\frac{E_y}{E_o} = e^{ikx} - \sum_{m=0}^{\infty} C_m i^m e^{-i\eta_m^*} \sin \eta_m^* H_m^{(1)'}(k\rho) (\cos m\phi \cos \phi) \quad (2)$$

For positive x, the term $(\cos m\phi \cos \phi)$ is unity. For negative x it has the value +1 for odd m and -1 for even m. Thus, points of negative x value can be obtained from the numerical data determined for the corresponding points of positive x value simply by changing the sign of even m terms, and changing the sign of the sin kx term in the exponential $e^{ikx}$.

The theoretical curves for points outside the 1 and $1\frac{1}{8}$ inch dielectric cylinders were calculated using equation (2) above, the British Association Mathematical tables being used for the Bessel functions $J_m$ and $Y_m$. The (Hankel function)' of the first kind $H_m^{(1)'}$ is given by

$$H_m^{(1)'} = J_m' + Y_m' \, i$$

where $J_o' = -J_1$

$$J_m' = \tfrac{1}{2}(J_{m-1} - J_{m+1}) \qquad m \neq 0$$

and $Y_o' = -Y_1$

$$Y_m' = \tfrac{1}{2}(Y_{m-1} - Y_{m+1}) \qquad m \neq 0$$

sin $\eta_m^*$ and cos $\eta_m^*$ were found from tan $\eta_m^*$ using the trigonometric tables from the Handbook of Chemistry and Physics and interpolating where necessary. The results of the calculations were squared to get the normalized intensity

$$\frac{I_y}{I_o} = \left| \frac{E_y}{E_o} \right|^2$$

An alternative method of evaluating equation (2) may be employed. The term $A_m = -\sin \eta_m^* \, e^{-i\eta_m^*}$ may be evaluated without recourse to the tan $\eta_m^*$ formula by direct evaluation of the following expression.

$$A_m = \frac{\left[J_m'(\bar{a})J_m(b) - \frac{1}{n} J_m(\bar{a})J_m'(b)\right] \left[\left(\frac{1}{n} J_m(\bar{a})J_m'(b) - J_m'(\bar{a})J_m(b)\right) - i\left(\frac{1}{n} Y_m(\bar{a})J_m'(b) - Y_m'(\bar{a})J_m(b)\right)\right]}{\left[\frac{1}{n} J_m(\bar{a})J_m'(b) - J_m'(\bar{a})J_m(b)\right]^2 \left[\frac{1}{n} Y_m(\bar{a})J_m'(b) - Y_m'(\bar{a})J_m(b)\right]^2} \qquad -(3)$$

where $\bar{a} = ka$, and $b = Nka$

In the case of the conducting cylinder

$$\eta_m^* \longrightarrow \delta_m'(ka)$$

where $\tan \delta'(x) = -J_m'(x)/Y_m'(x)$

It was found that the series had to be calculated as far as ten terms for points near the surface of the cylinders. For points further out, six or eight terms were quite sufficient for proper convergence of the series.

The expression for points inside the dielectric cylinder ($\rho<a$) is as follows.

$$\frac{E_y}{E_o}=\sum_{m=0}^{\infty} C_m\, i^{m-1}\, B_m\left[\frac{1}{n}\cos m\phi\,\cos\phi\; J_m'(Nk\rho)+\frac{m}{n^2 k\rho}\sin m\phi\,\sin\phi\; J_m(Nk\rho)\right] \qquad -(4)$$

where the factor $B_m$ is given in full by

$$B_m=\frac{\frac{2}{\pi k a}\left[\left(J_m'(a)J_m(b)-\frac{1}{n}J_m(a)J_m'(b)\right)+i\left(\frac{1}{n}Y_m(a)J_m'(b)-Y_m'(a)J_m(b)\right)\right]}{\left[\frac{1}{n}J_m(a)J_m'(b)-J_m'a)J_m(b)\right]^2+\left[\frac{1}{n}Y_m(a)J_m'(b)-Y_m'(a)J_m(b)\right]^2} \qquad -(5)$$

For the case under consideration (i.e. $y=0,\pi$), equation (4) reduces to the form

$$\frac{E_y}{E_o}=\sum_{m=0}^{\infty} C_m\, i^{m-1}\, B_m\,\frac{1}{n}\,J_m'(Nk\rho)(\cos m\phi\,\cos\phi) \qquad (6)$$

where the factor ($\cos m\phi\,\cos\phi$) has the same properties of sign as mentioned previously.

The values for points inside the cylinders, as presented in Figs. 12 and 14, were calculated from equation (6) using expression (5) for the determination of $B_m$. Hence, it would have been expedient in the long run to evaluate the points outside the cylinders by use of expression (3) rather than by direct use of equation (2) of Froese and Wait.

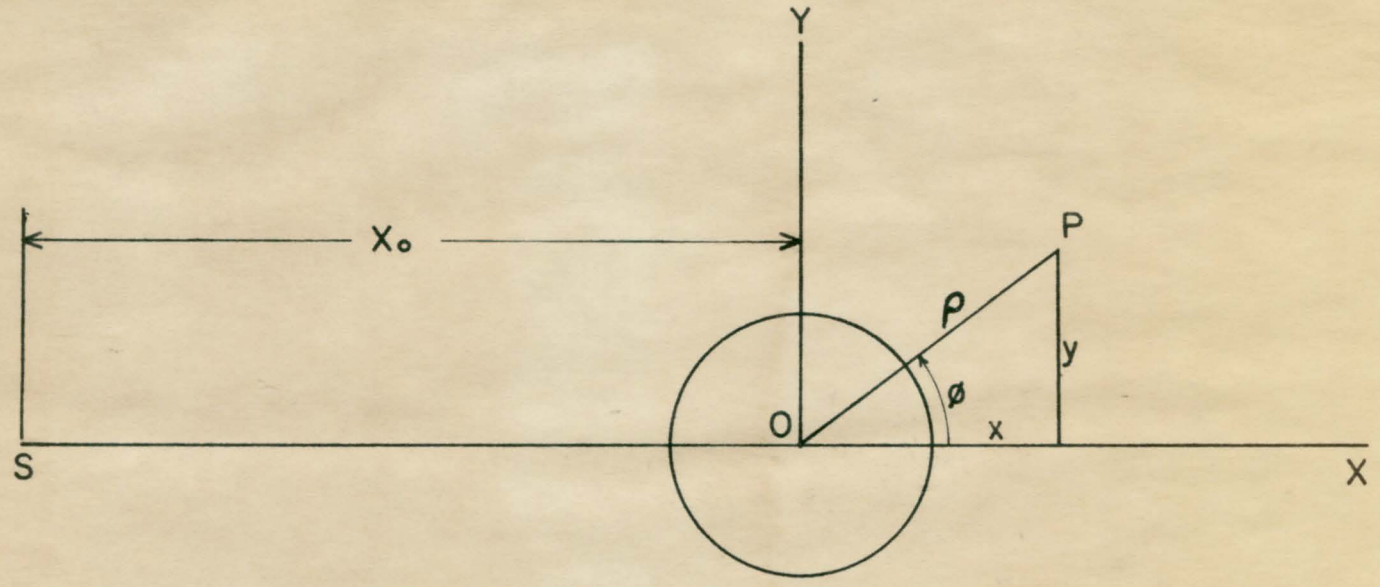


FIG. 20: GEOMETRY OF DIFFRACTION EXPERIMENT

## LIST OF REFERENCES


| NO. | REFERENCE |
|---|---|
| 1. | Wiles, S. T. and McLay, A. B., Can. Jour. Phys., 32: 372. 1954. |
| 2. | Keys, J. E., Diffraction of Microwaves, M.Sc. Thesis, McMaster University, October 1953. |
| 3. | Froese, C. and Wait, J. R., Can. Jour. Phys., 34: 775 1954. |
| 4. | Subbarao, M. K. and McLay, A. B., Can. Jour. Phys., 34: 546. 1956. |
| 5. | Subbarao, M. K. and McLay, A. B., Can. Jour. Phys., 34: 555. 1956. |
| 6. | Jordan, C. E. and McLay, A. B., Can. Jour. Phys., 35: 1253. 1957. |
| 7. | Jordan, C. E., Total Reflection of Microwaves by a Prism and Semicylinder, M.Sc. Thesis, McMaster University, October 1960. |
| 8. | Dignum, R., Dielectric Constant Measurements and Also Microwave Optics of a Prism, M.Sc. Thesis, McMaster University, April 1960. |
| 9. | Hedgecock, N. E., Microwave Optics of a Prism, M.Sc. Thesis, McMaster University, April 1959. |
| 10. | Leung, P., Microwave Optics of a Prism, M.Sc. Thesis, McMaster University, October 1961. |
| 11. | Kneeland, D. R., Refraction and Total Reflection of Microwaves by a Prism, M.Sc. Thesis, McMaster University, October 1954. |